

Models of Metal-Poor Stars with Different Initial Abundances of C, N, O, Mg, and Si. I. Bolometric Corrections Derived from New MARCS Synthetic Spectra and Their Implications for Observed Colour-Magnitude Diagrams

Don A. Vandenberg,^{1*} Bengt Edvardsson,² Luca Casagrande,³ and Jason W. Ferguson⁴

¹*Department of Physics and Astronomy, University of Victoria, P.O. Box 1700, STN CSC, Victoria, BC, Canada V8W 2Y2*

²*Theoretical Astrophysics, Department of Physics & Astronomy, Uppsala University, Box 516, SE-751 20 Uppsala, Sweden*

³*Research School of Astronomy and Astrophysics, Mount Stromlo Observatory, The Australian National University, Canberra, A.C.T. 2611, Australia*

⁴*Department of Physics, Wichita State University, Wichita, KS 67260-0032, U.S.A*

Accepted XXX. Received YYY; in original form ZZZ

ABSTRACT

New, high-resolution MARCS synthetic spectra have been calculated for more than a dozen mixtures of the metals allowing, in turn, for variations in C:N:O, [CNO/Fe], and enhanced abundances of C, O, Mg, and Si. Bolometric corrections (BCs) for many of the broad-band filters currently in use have been generated from these spectra. Due to improved treatments of molecules that involve atoms of C, N, and O, the BCs for UV and blue passbands, in particular, differ substantially from those derived from previous MARCS models. These differences, and the effects on the BCs of varying the abundances of the metals, are shown in a number of instructive plots. Stellar evolutionary grids for $-2.5 \leq [\text{Fe}/\text{H}] \leq -0.5$ have also been computed for the different mixtures. Isochrones based on these tracks are intercompared on the theoretical H-R diagram and on a few of the colour-magnitude diagrams that can be constructed from *HST* Wide Field Camera 3 (WFC3) *F*336W, *F*438W, *F*606W, *F*814W, *F*110W, and *F*160W observations. For the first application of these models, isochrones have been fitted to WFC3 photometry of the globular cluster NGC 6496 from the *HST* UV Legacy Survey, with very encouraging results.

Key words: globular clusters: individual: NGC 6496 — stars: abundances – stars: evolution – stars: Population II – Hertzsprung-Russell and colour-magnitude diagrams

1 INTRODUCTION

Hubble Space Telescope (*HST*) Wide Field Camera 3 (WFC3) observations of globular clusters (GCs) are yielding spectacular colour-magnitude diagrams (CMDs) that reveal the presence of chemically distinct, multiple stellar populations (MSPs) within them to an unprecedented degree; see, e.g., the recent studies of NGC 2808 (Milone et al. 2015a), M2 (Milone et al. 2015b), ω Cen (Bellini et al. 2017), and NGC 2419 (Zennaro et al. 2019). Indeed, the *HST* UV Legacy Survey (Piotto et al. 2015, Nardiello et al. 2018) was designed to use just five filters (*F*275W, *F*336W, *F*438W, *F*606W, and *F*814W) to identify stars with different abundances of He, C, N, and O. Complementary investigations of lower main-sequence (LMS) stars in the IR have also been used to differentiate between them in terms of their oxygen contents (e.g., Milone et al. 2017, Milone et al. 2019), and to determine the cluster

distances, and hence ages (e.g., Di Cecco et al. 2015, Massari et al. 2016, Correnti et al. 2018, Saracino et al. 2018).

To be sure, the *existence* of the MSPs that reside in GCs was already well established as the result of the enormous amount of spectroscopic work that has been carried out since the middle of the last century. Spectra of cluster giants revealed early on that there are star-to-star variations in the strengths of the CN bands (Popper 1947, Osborn 1971) and the abundances of Na (Cohen 1978, Peterson 1980), Mg (Pilachowski 1989, Shetrone 1996a), and Al (Norris et al. 1981). Moreover, the strengths of some spectral features were found to be either correlated or anti-correlated with the strengths of other features; e.g., CN-strong stars have larger Na and Al abundances, but smaller O abundances, than CN-weak stars (Norris & Pilachowski 1985, Sneden et al. 1991, Drake et al. 1992, Brown & Wallerstein 1992). For many years it was debated (see, e.g., the review by Kraft 1994) whether the derived abundances were primordial in nature or due primarily to nucleosynthesis and

* E-mail: vandenberg@uvic.ca

mixing processes within the stars, given that the targets of these studies were highly evolved giants.

To try to resolve this issue, Hesser (1978) observed lower red-giant branch (RGB) stars in 47 Tuc, finding that CN variations persisted to at least $M_V \sim +3$. Hesser & Bell (1980) then determined that the variation of CN strengths in several upper MS stars in the same cluster was comparable to that seen in bright giants, which argued in support of the possibility that the stars formed out of material with nonuniform ratios of C:N:O — unless deep mixing can occur relatively close to the turnoff (TO). Many subsequent studies over the next two decades showed that it is a common property of TO and upper MS stars in GCs that they exhibit variations in CN, O, Na, Mg, and Al, though the amplitudes of such variations vary from cluster to cluster (e.g., Cannon et al. 1998, Gratton et al. 2001, Ramírez & Cohen 2003, Cohen et al. 2005 Carretta et al. 2009b). This left little doubt that the gas out of which the cluster stars formed must have been chemically inhomogeneous — although their surface abundances are subsequently altered to some extent by diffusive processes during MS evolution (e.g., Richard et al. 2002, Vandenberg et al. 2002, Dotter et al. 2017) and by deep mixing along the upper RGB (e.g., Carbon et al. 1982, Pilachowski 1988, Denissenkov & Vandenberg 2003). More recent advances include the determination of Mg isotopic ratios (Shetrone 1996b, Yong et al. 2003, Yong et al. 2006) and the discovery of the Al–Si correlation (Yong et al. 2005), which are both indicative of p -capture nucleosynthesis at very high temperatures.

It is likely to be several years before reliable quantitative measurements of light element abundances will be obtained from photometry because bolometric corrections (BCs), at short wavelengths in particular, require that the synthetic spectra from which they are calculated take into account all of the important sources of opacity due to atomic lines and molecular bands. This is a huge, ongoing challenge, especially in the UV. Contributing to this problem are the uncertainties associated with the stellar T_{eff} scale, which appear to be at the level of ~ 70 – 100 K for upper MS and TO stars (Casagrande et al. 2010), but undoubtedly much higher than this for the coolest dwarfs and giants. Also of considerable importance are the uncertainties connected with the microturbulence, which is used as a free parameter in one-dimensional model atmospheres to broaden spectral lines in order to take into account small-scale motions generated by atmospheric convection. Because the microturbulence has the effect of redistributing the flux in spectral regions that are crowded with lines, it can affect BCs in some passbands by several hundredths to a few tenths of a magnitude, depending on the temperature and metallicity (Casagrande & Vandenberg 2014, hereafter CV14; see their Figs. 3 and 4). (The fluxes computed from 3D model atmospheres are not subject to this limitation as they are derived from the modeling of convective motions and turbulent flows; see, e.g., Bonifacio et al. 2018, Chiavassa et al. 2018.) The superb CMDs from the UV Legacy Survey (Nardiello et al. 2018) will clearly be an invaluable resource for the testing and improvement of synthetic colour– T_{eff} relations that are used by isochrones to interpret these observations.

A possible indication of the deficiencies of current stellar models and synthetic spectra is the finding by Milone et al. (2018) that the helium abundances derived from so-called “chromosome maps” (Milone et al. 2015a), which use a specific combination of UV and optical colour indices to provide a clear separation of stars with different chemical compositions, do not agree with the abundance variations that have been inferred from theoretical sumu-

lations of horizontal-branch (HB) populations in GCs.¹ For instance, the latter deduced that $\delta Y \gtrsim 0.10$ in M3 from the length of the sequence of stars in the chromosome map that they ascribe to first-generation stars, whereas they obtained $\delta Y_{\text{max}} = 0.004 \pm 0.011$ for NGC 6362. This is in stark contrast with the results of Denissenkov et al. (2017), who found a very good match between the predicted and observed HB of M3 if $\delta Y \sim 0.01$ and the models assume a moderate amount of mass loss along the giant branch. [A follow-up study of M3 by Tailo et al. (2019) also concluded that the large spread in Y derived from the chromosome map was incompatible with the cluster HB morphology, the period and luminosity distribution of its RR Lyrae, and the colour distribution of its MS stars.] In the case of NGC 6262, the difference in luminosity between the non-variable HB stars on either side of the instability strip, as well as simulations of the entire HB population, imply $\delta Y \sim 0.03$ (Vandenberg & Denissenkov 2018). It would appear that our understanding of chromosome maps, or of GCs, is lacking in some fundamental way.

During the past several decades, many studies have examined the effects on stellar models of varying the assumed metal abundances. For instance, variations in O were considered by Rood & Crocker (1985) and Vandenberg (1992), while differences in the abundances of the α -elements as a group were studied by Salaris et al. (1993), Vandenberg et al. (2000), Pietrinferni et al. (2006), and Dotter et al. (2007), among others. Vandenberg et al. (2012, also see Beom et al. 2016) computed isochrones for metal-deficient stars in which 10 of the most abundant metals from C to Ti were enhanced by 0.4 dex, in turn, at constant [Fe/H]. Colour– T_{eff} relations for different choices of $[\alpha/\text{Fe}]$ have been generated by CV14 (also see Cassisi et al. 2004) for large ranges in $\log g$, $\log T_{\text{eff}}$, and [Fe/H], based on MARCS model atmospheres and synthetic spectra (Gustafsson et al. 2008). Investigations of the consequences of C–N–O–Na–Mg–Al correlations and anticorrelations for isochrones and their transformations to various CMDs were undertaken by Salaris et al. (2006), Pietrinferni et al. (2009), Sbordone et al. (2011), and Cassisi et al. (2013). This brief mention of just a few of the papers that have dealt with stellar abundances from a theoretical perspective is sufficient to show that the most basic questions concerning the impact of abundance variations have already been addressed. It seems likely that further advancements will mainly occur as a result of refinements to model atmospheres, synthetic spectra and the associated BCs, and the T_{eff} scale of stellar evolutionary computations.

Because the CV14 transformations, coupled with Victoria-Regina isochrones (Vandenberg et al. 2014) have had considerable success reproducing optical and near-IR CMDs of GCs (see, e.g., Vandenberg et al. 2013, hereafter VBLC13; Correnti et al. 2016), we decided to compute new synthetic spectra that take various abundance variations into account, to calculate BCs from those spectra for a large fraction of the broad-band filters currently in use, including the *HST* WFC3 filters, and to generate new isochrones for the assumed abundances. It turns out that the improvements which have been made by the Uppsala group to the MARCS spectral synthesis code since the study by Gustafsson et al. (2008) — primarily to the treatment of molecules involving C, N, and O — have

¹ This problem does raise any doubts about the very high He abundance that has been deduced for the blue MS stars in ω Cen (Piotto et al. 2005), which is arguably the most important, and the most surprising, discovery in the stellar populations research area in recent years. Isochrones appear to be able to fit the CMD locations of these stars only if they assume $Y \sim 0.4$ (see, e.g., King et al. 2012, Herwig et al. 2012).

Table 1. The Adopted Chemical Abundances and the Associated BC Tables

Names of BC Tables ^a	He	C	N	O	[CNO/Fe]	Mg	Si	v_T^b
a4s08	10.93	8.39	7.78	9.06	+0.28	7.93	7.91	2.0
a4s21	11.00	8.43	7.83	9.09	+0.28	8.00	7.91	f(g)
a4CN	–	↓ 0.3	↑ 0.50	–	+0.28	–	–	f(g)
a4CNN	–	↓ 0.3	↑ 1.13	–	+0.44	–	–	f(g)
a4ON	–	↓ 0.8	↑ 1.30	↓ 0.8	+0.28	–	–	f(g)
a4ONN	–	↓ 0.8	↑ 1.48	↓ 0.8	+0.44	–	–	f(g)
a4xC_p4	–	↑ 0.4	–	–	+0.38	–	–	f(g)
a4xCO	–	↑ 0.7	–	↑ 0.2	+0.61	–	–	f(g)
a4xO_p2	–	–	–	↑ 0.2	+0.44	–	–	f(g)
a4xO_p4	–	–	–	↑ 0.4	+0.62	–	–	f(g)
a4Mg_p2	–	–	–	–	+0.28	↑ 0.2	–	f(g)
a4Si_p2	–	–	–	–	+0.28	–	↑ 0.2	f(g)
s08std	10.93	8.39	7.78	8.66	0.00–0.28 ^c	7.53	7.51	2.0
s08vt1	–	–	–	–	–	–	–	1.0
s08vt5	–	–	–	–	–	–	–	5.0
s21std	–	–	–	–	–	–	–	f(g)
s21Y30	11.04	–	–	–	–	–	–	f(g)

^a Boldface font identifies reference models (see the text); the others involve changes to the abundances of one or more of the metals, as tabulated, or to v_T . Only the “a4” BCs are used to transform isochrones to various CMDs; the others are employed by codes that are provided (see the Data Availability section) to evaluate, and to present in tabular form, the effects on BCs of varying the microturbulence or the assumed helium abundance.

^b f(g) implies that the microturbulent velocity, v_T , varies with gravity such that $v_T = 1.0$ km/s if $\log g \geq 4.0$ or 2.0 km/s if $\log g \leq 3.0$.

^c The specified range in [CNO/Fe] corresponds to an increase in [O/Fe] from 0.0 at [Fe/H] = 0.0 to 0.4 at [Fe/H] = –1.0 (see the text).

very significant consequences for the BCs that are calculated for UV filters but rather little impact on the those at optical and longer wavelengths. However, as noted by Edvardsson (2008), MARCS model fluxes are less reliable in the blue spectral region due to the importance of, and uncertainties associated with, the continuous non-hydrogenic opacities at shorter wavelengths.

The main goal of this series of papers is to examine how well isochrones that employ the improved BCs are able to reproduce observed GC CMDs that involve colours ranging from $m_{F336W} - m_{F438W}$ to $m_{F110W} - m_{F160W}$. Unfortunately, the synthetic spectra do not extend far enough into the UV to permit the calculation of BCs for the $F275W$ filter, which was selected for the *HST* UV Legacy Survey to distinguish between stars with different O abundances because this passband contains an OH band; see Piotto et al. 2015. In this paper, we describe and discuss the assumed heavy-element mixtures and their consequences for both the BCs and stellar evolutionary models. Comparisons of our isochrones with WFC3 observations of GCs that span a wide range in [Fe/H] are presented in Paper II.

2 THE CALCULATION OF BOLOMETRIC CORRECTIONS

2.1 The Assumed Chemical Abundances

Table 1 lists the $\log N_i$ number abundances, on the scale $\log N_H = 12.0$, of just those elements for which abundance variations have been considered in this investigation. The two reference models (in boldface font) assume the solar abundances reported by Grevesse et al. (2007), which were adopted in the generation of large grids of MARCS model atmospheres and synthetic spectra by Gustafsson et al. (2008). Whereas a4s08 takes into account a 0.4

dex enhancement of all of the α elements (O, Mg, and Si, as well as Ne, S, Ca, and Ti, even though they are not explicitly included in the table), s08std assumes that $[\alpha/\text{Fe}] = +0.4$ at $[\text{Fe}/\text{H}] \leq -1.0$, with a linear decrease from 0.4 at $[\text{Fe}/\text{H}] = -1.0$ to 0.0 at $[\text{Fe}/\text{H}] = 0.0$ (a pattern that is roughly characteristic of local Galactic disk and halo stars; e.g., Edvardsson et al. 1993). In the case of the a4s08 models, the abundances of all of the metals at a given metallicity can be obtained simply by adding the [Fe/H] value to the tabulated $\log N_i$ values. For the s08std models, the abundances of the α elements must first be increased by the relevant value of $[\alpha/\text{Fe}]$ (e.g., 0.3 dex if considering stars with $[\text{Fe}/\text{H}] = -0.75$) before the abundances of all of the metals are scaled to the metallicity of interest ($[\text{Fe}/\text{H}] = -0.75$ in our example).

In order that the computed grids of evolutionary tracks and isochrones be consistent with those reported by VandenBerg et al. (2014), which allow for variations in $[\alpha/\text{Fe}]$ over wide ranges in [Fe/H] and Y , we decided to adopt the elemental abundances given by Asplund et al. (2009) as the base mixture, instead of Grevesse et al. (2007). Thus, in Table 1, the name a4s21 has been given to the mixture of the metals reported by Asplund et al. with a 0.4 dex enhancement of the α elements. Note that “a4” implies that “[α/Fe] = +0.4” in the base mixture and that the numbers “08” or “21” in the names identify, in turn, the 2008 or 2021 MARCS models. To examine the impact of varying C, N, O, Mg, and Si, the a4s21 abundances have been modified in a number of different ways by amounts that are described by upward- or downward-pointing arrows followed by the adopted values of $\delta \log N_i$.

The assigned names of the different variations were chosen to make it easy to remember them. For instance, for typical scaled-solar abundances of C and N, the CN abundance reaches a maximum value due to CN-cycling when C has been reduced by ~ 0.3 dex (see, e.g., Smith 1987, his Fig. 8), which then requires that N be

enhanced by ~ 0.5 dex if $C+N = \text{constant}$. Just as a4CN is a reasonable label for this case, a4CNN is a suitable name for a mixture that assumes the same depletion of C but a higher N abundance. Similarly, predictions of ON-cycling by, e.g., Denissenkov & Weiss (2004) are able to explain the very low C and O abundances ($[C/Fe] \sim -0.8$, $[O/Fe] \sim -0.4$) that have been derived spectroscopically in some GC stars (see, e.g., Smith et al. 1996, Cohen et al. 2002). Accordingly, a mixture of the metals in which the a4s21 abundances of C and O have been depleted by 0.8 dex, and N increased by an amount such that $C+N+O = \text{constant}$, has been given the name a4ON, while a4ONN refers to a mixture having the same depletions of C and O but a higher N abundance — to be consistent with a higher value of $[CNO/Fe]$. Spectroscopic work over the years has established that values of $[N/Fe] \sim +1.5$ are typically found in GCs; see Briley et al. (2004), Smith et al. (2005), Cohen et al. (2005).

As α -enhanced Population II stars appear to have $[C/Fe] > 0$ (specifically, $[C/Fe] \approx 0.2$; see Nissen et al. 2014), we opted to consider two cases with increased C abundances; specifically, a4xC_p4, which assumes a 0.4 dex enhancement, and a4xC0, which considers higher abundances of both C and O by 0.7 dex and 0.2 dex, respectively. When the abundances of single elements are altered, we have adopted the convention wherein the symbol for the element is followed by “_p”, where “p” represents “+” and the number after the “p” gives the enhancement in tenths of a dex. Granted, these abundances of carbon are much higher than those derived in current observational studies of GCs (see, e.g., Carretta et al. 2005), though high C is suggested by anomalous populations of CO-strong stars in some systems (notably ω Cen; see Norris & Da Costa 1995, and references therein). (The determination of whether or not $[C/Fe]$ varies with $[Fe/H]$ depends quite sensitively on the adopted T_{eff} scale and on the importance of non-LTE effects, as shown in the study of metal-poor field stars by Fabbian et al. 2009.) In addition, Paper II provides some tantalizing evidence that GCs may contain sub-populations of stars with unusually high C enhancements; consequently, there is ample justification for studying the a4xC_p4 and a4xC0 cases. The remaining mixtures that we have considered allow for 0.2 and 0.4 dex enhancements of oxygen (a4x0_p2 and a4x0_p4, respectively), as well as enhanced Mg by 0.2 dex (a4Mg_p2) and increased Si abundances by 0.2 dex (a4Si_p2).²

Although the BCs for the “a4” mixtures have been newly com-

² During the course of this investigation, we found that the effects on BCs of an enhanced Mg abundance by 0.2 dex were significantly larger than those obtained by increasing the abundances of all of the α elements by 0.2 dex. B.E. and his colleague at Uppsala Observatory, K. Eriksson, studied this difficulty and found that it occurred because of an assumption that was made when considering modest abundance enhancements of single elements. Normally, synthetic spectra are based on fully consistent model atmospheres. However, in the case of Mg, the model atmosphere structures were initially assumed to be the same with, or without, the 0.2 dex enhancement in its abundance; i.e., the abundance difference was treated only in the calculation of the synthetic spectra. When B.E. and K.E. computed model atmospheres for enhanced Mg and based the synthetic spectra on these atmospheres, the resultant BCs were much more consistent with those obtained when the abundances of all of the α elements as a group were increased by the same amount. This is potentially a very important finding that should be thoroughly studied. The BCs at short wavelengths, in particular, where there is little flux in the case of cool giants and MS stars, are unlikely to be very trustworthy unless they are based on fully consistent model atmospheres and synthetic spectra. Indeed, it is possible that similar consistency may be necessary when determining stellar abundances from fits to observed spectral features; at least, this is a concern that war-

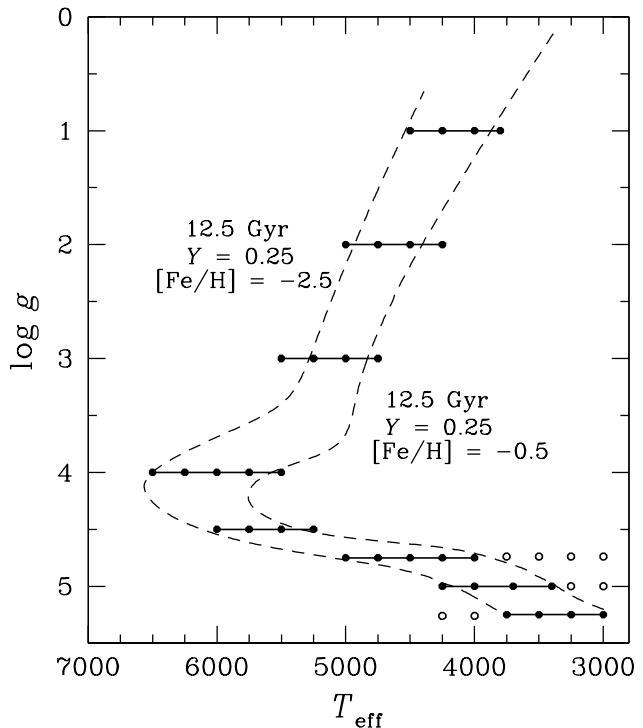


Figure 1. A T_{eff} , $\log g$ diagram that gives the effective temperatures and gravities (the filled circles) for which MARCS model atmospheres and synthetic spectra have been computed. The horizontal solid lines specify the ranges in T_{eff} at the adopted $\log g$ values; they match quite well the differences in T_{eff} predicted by Victoria-Regina isochrones (Vandenberg et al. 2014) for the indicated ages and chemical compositions (the dashed loci). Additional model atmospheres for use as atmospheric boundary conditions in the stellar models of low-mass stars were computed for the T_{eff} , $\log g$ values that are represented by small open circles.

puted specifically for this investigation, using the same formalism, zero-points, and filter transmission curves of CV14, those for the a4s08 and s08std cases have been derived from the tables given by CV14 using their software. These BCs assume a microturbulent velocity, v_T , of 2.0 km/s whereas the default assumption for MARCS models, including the current ones in the “a4” series, is to adopt 1.0 km/s if $\log g \geq 4.0$ and 2.0 km/s if $\log g \leq 3.0$. This implications of this difference for computed BCs are discussed in § 3.

The “a4” computations also assume $\log N_{\text{He}} = 11.0$, or $Y \approx 0.28$. Unlike the metals, helium contributes very little to the opacities in the surface layers of lower-mass stars, though higher Y does make the gas slightly more transparent by diluting the electron density and the metals. Its main effect is to increase the mean molecular weight, which compresses the atmosphere somewhat, thereby mimicking an atmosphere with a higher gravity. As reported by Girardi et al. (2007), and confirmed by a number of computations that we have carried out for $Y = 0.25$ (s21std) and $Y = 0.30$ (s21Y30), moderate He abundance variations do not affect the BCs for broad-band filters by more than a few to several thousandths of a magnitude; consequently, it is not necessary to generate BC tables for different values of Y , especially for an exploratory study such as ours.

rants careful consideration. As a result of this discovery, all of our synthetic spectra are based on fully consistent model atmospheres.

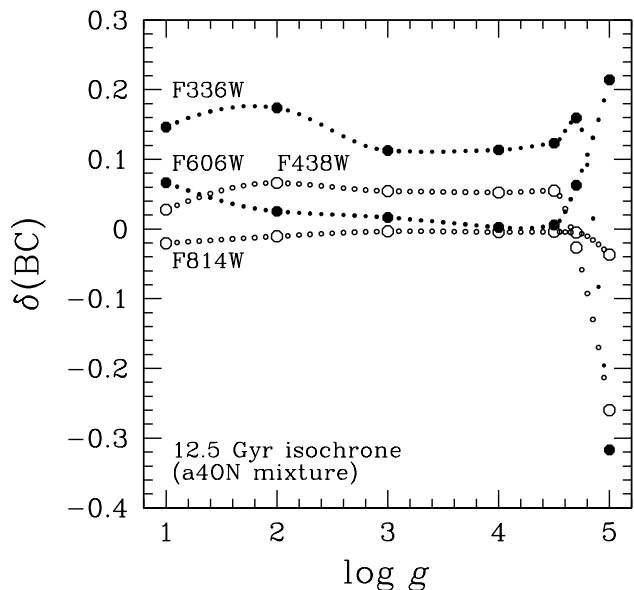


Figure 2. The differences between the BCs for the a40N mix and those given by CV14 for the (a4s08) reference models at the T_{eff} values predicted by a 12.5 Gyr isochrone for $[\text{Fe}/\text{H}] = -0.5$ and the a40N mix at $\log g = 1.0, 2.0, 3.0, 4.0, 4.5, 4.7,$ and 5.0 (the large filled and open circles). The smaller circles were obtained by interpolating between the larger ones using Akima splines (see the text).

2.2 The Adopted Parameter Variations

The calculation of high-resolution spectra for wide ranges in $\log g$, T_{eff} , and $[\text{Fe}/\text{H}]$ becomes an especially computationally demanding project if many different mixtures of the heavy elements are also considered. In order to make the BC computations more manageable, they have been limited to the $\log g$ and T_{eff} values that are indicated by the filled circles in Figure 1. As shown in this figure, the adopted temperatures were determined from a consideration of the differences in T_{eff} , at the selected gravities, between isochrones relevant to old stellar populations with $[\text{Fe}/\text{H}] = -2.5$ and -0.5 . However, even with these restrictions, it was necessary to generate over 1100 model atmospheres and synthetic spectra — for 34 $T_{\text{eff}}, \log g$ values at each of three metallicities ($[\text{Fe}/\text{H}] = -2.5, -1.5,$ and -0.5) and each of the 11 “a4” mixtures that are listed in Table 1). As the spectra were calculated for $R > 225,000$, where R is the ratio of the wavelength to the step in wavelength at which the fluxes are evaluated, spectral features are very well resolved.

In general, the effects on BCs for broad-band filters of varying the abundances of a small subset of the metals are not very large at $\log g \lesssim 4.7$. Moreover, the variations of the differences in the BCs that are obtained with, and without, the changes to the mixtures of the metals considered here tend to be smooth, well-behaved functions of $\log g$ that can be interpolated to quite high accuracy. Even at $\log g > 4.7$, where such differences tend to increase quite rapidly, the loci connecting the $\delta(\text{BC})$ values at $\log g = 4.5$ and 5.0 appear to be quite well constrained by the results at $\log g = 4.7$.

These claims are supported by Figure 2, which plots, for four of the WFC3 filters, the differences in the BCs for the a40N mix and those given by CV14 for the relevant reference mix (a4s08) at the fiducial $\log g$ values. To be more specific, both sets of BCs were derived for the temperatures and gravities along a 12.5 Gyr isochrone for $[\text{Fe}/\text{H}] = -0.5$ and the a40N mixture, for which the $\delta(\text{BC})$ variations are comparable to, or larger, than those predicted

for most of the mixtures listed in Table 1. Interpolations via Akima splines (Akima 1970), which were fitted to the large filled and open circles at the grid values of $\log g$, yielded the smaller circles at intermediate gravities. Even when the $\delta(\text{BC})$ values change by a relatively large amount — as in the BCs for the $F336W$ filter between $\log g = 4.7$ and 5.0 (see Fig. 2) — the interpolated points still look very reasonable.

To predict the consequences of the different metal abundance variations on a given CMD, we have therefore opted to use the following procedure. First, isochrones for the revised mixture (e.g., a40N) are transposed to the selected CMDs using the CV14 BCs for the a4s08 reference mix, which cover much wider ranges in $[\text{Fe}/\text{H}]$, T_{eff} , and $\log g$, at a significantly higher resolution, than the BC tables that were generated for this study. Second, the differences between the CV14 BCs at $\log g = 1.0, 2.0, \dots, 5.0$, at the isochrone T_{eff} values, and those for the revised mix are evaluated, and Akima splines are fitted to the resultant $\delta(\text{BC})$ values (as in Fig. 2). The last step is simply to use the Akima splines to correct the CV14 BCs at each of the isochrone points with gravities in the range $1.0 \leq \log g \leq 5.0$. Extrapolations to lower or higher values of $\log g$ are carried out, as necessary, using quadratic equations that describe the variations of $\delta(\text{BC})$ with gravity at $\log g = 1.2, 1.1,$ and 1.0 or at $\log g = 4.9, 4.95,$ and 5.0 , using the interpolated $\delta(\text{BC})$ at other than the grid values of $\log g$.

Figure 3 illustrates the results that are obtained for the same 12.5 Gyr isochrone for the a40N mixture that was considered in the previous figure. The dashed loci in each panel represents the isochrone when it is transposed to three of the CMDs that are considered in our analyses of GC observations in Paper II using CV14 BCs for the $F336W$, $F438W$, $F606W$, and $F814W$ filters. The solid curves are obtained if the differences between the CV14 and the a40N BCs, as derived from Akima spline interpolations (Fig. 2) and quadratic extrapolations, are applied to the CV14 transformations. For the most part, the offsets are quite small and they reflect the behavior of the $\delta(\text{BC})$ variations with $\log g$ in the previous figure; e.g., the cross-over of the $\delta(\text{BC})$ values for $F438W$ and $F606W$ filters translates to a cross-over of the $M_{F438W} - M_{F606W}$ colours at $\log g \sim 1.4$ and ~ 4.6 .³

3 THE EFFECTS OF CHEMICAL ABUNDANCE VARIATIONS ON BOLOMETRIC CORRECTIONS

To illustrate some of the properties of the different BC transformations, we decided to plot histograms of the differences in the BCs that have been derived for several of the cases in Table 1 at common values of $\log g$, T_{eff} , $[\text{Fe}/\text{H}]$, and $[\alpha/\text{Fe}]$. In fact, we have adopted $\delta(\text{magnitude}) = -\delta(\text{BC})$ for the ordinate in order to better relate the results to observed stars. In addition, we opted to consider the Johnson-Cousins-2MASS $UBVI_CK_S$ passbands along with seven of the WFC3 filters, ranging from $F336W$ in the UV to $F160W$ in

³ Although BCs were generated for $\log g = 5.3$ (see Fig. 1), it turns out that stellar models for Pop. II stars with such gravities are very close to the H-burning limit, where the equation of state that we use for low-mass stars, FreeEOS (<http://freeeos.sourceforge.net>) is known to have convergence difficulties. Indeed, for some of the metal abundance mixtures, we were unable to obtain converged MS models with sufficiently low masses ($\lesssim 0.1 M_{\odot}$) in order to reach $\log g \geq 5.3$. However, it is clear from Fig. 3 that the extensions of our isochrones to $\log g = 5.0$ already extend to $M_{F606W} \sim 11.5$, which is more than adequate for the comparisons with observations that are presented in Paper II.

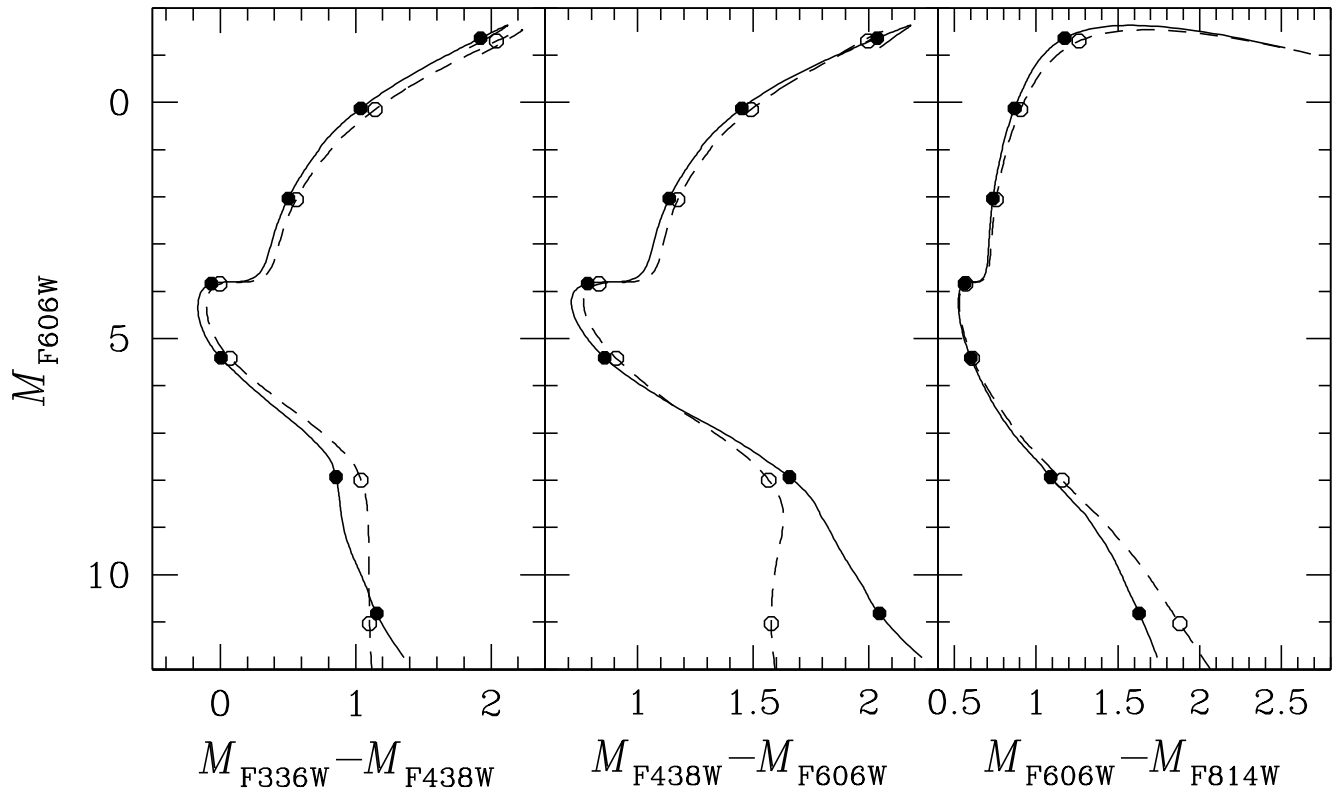


Figure 3. Transformation of a 12.5 Gyr isochrone for $[\text{Fe}/\text{H}] = -0.5$ and the a40N mixture to three CMDs using CV14 BCs for the standard a4s08 mix (dashed curves) and the adjusted BCs that are derived from the $\delta(\text{BC})$ offsets shown in Fig. 2 (solid curves). The large open and filled circles identify the points along the isochrones at the fiducial $\log g$ values (1.0, 2.0, ..., 5.0).

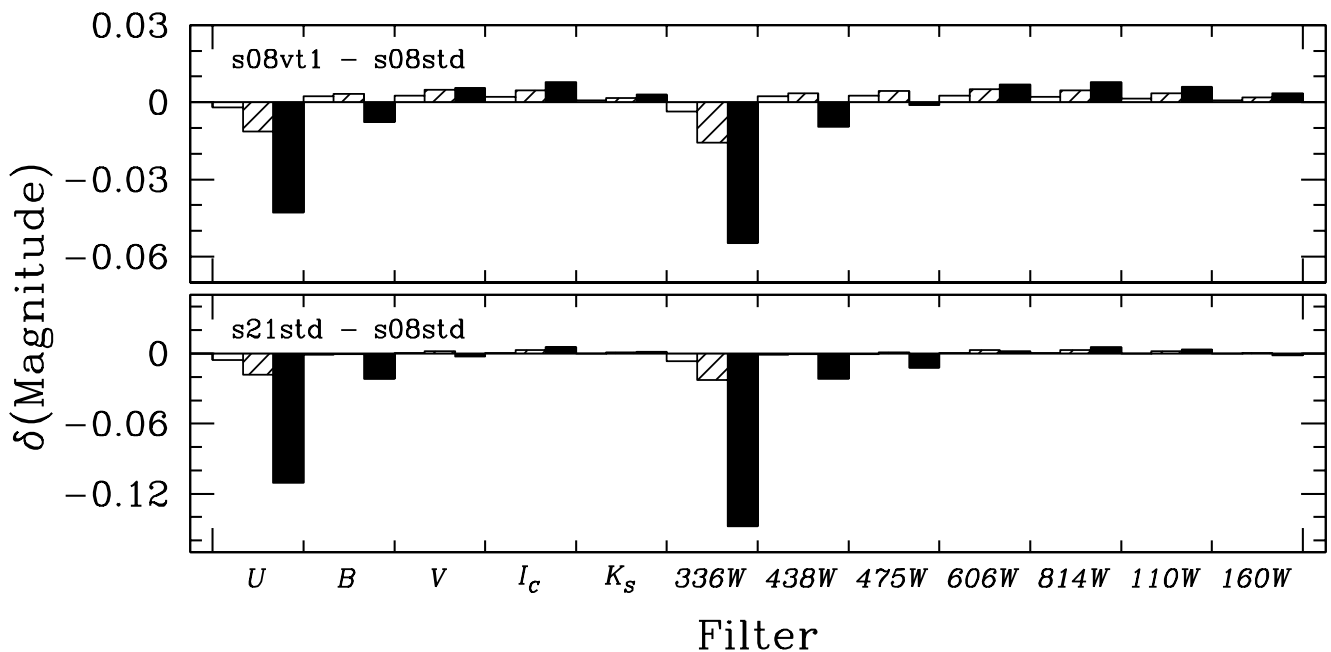


Figure 4. *Top Panel:* Histogram showing the predicted magnitude change in passbands ranging from U to F160W if the MARCS models assume a microturbulent velocity, v_t , of 1 km/s (s08vt1 in Table 1) instead of 2 km/s (s08std). The open, hatched, and filled vertical bars associated with each filter represent the predictions for $[\text{Fe}/\text{H}] = -2.5, -1.5,$ and -0.5 , respectively. The models assume $\log g = 4.0$ and the T_{eff} s from 12.5 Gyr isochrones at this gravity and the relevant metallicity; specifically $T_{\text{eff}} = 6499, 6162,$ and 5576 K, in turn. (The "F" in "F336W" and in each of the other WFC3 filter names has been omitted for the sake of clarity.) *Bottom panel:* Similar to the top panel, except that the differences between the BCs calculated for the s21std and s08std models are shown. Note that a difference in the assumed microturbulent velocity contributes to the differences arising from improvements to the MARCS codes.

the IR, in order to sample the synthetic spectra over nearly the full range in wavelength for which they were computed. (The *HST* filters are of particular interest given that comparisons of isochrones with WFC3 observations of GCs are presented in the penultimate section of this paper as well as in Paper II.) Examples of the histograms are shown in Figure 4; the three vertical bars that are plotted for each filter indicate the differences in the predicted magnitudes between the *s08vt1* and *s08std* BCs (top panel), and between the *s21std* and *s08std* BCs (bottom panel) for $[\text{Fe}/\text{H}] = -2.5, -1.5, \text{ and } -0.5$, in the direction from left to right. These results assume $\log g = 4.0$, which is approximately the gravity of TO stars, and the T_{eff} s given in the figure caption.

Because the 2008 MARCS models for $v_T = 1.0$ km/s and 5.0 km/s were generated only for limited ranges in gravity, it is not possible to use the BCs based on these models to transform entire isochrones from the MS to the RGB tip to the observed plane. Nevertheless, the differences in the BCs caused by a decrease in v_T from 2.0 km/s to 1.0 km/s or an increase from 2.0 km/s to 5.0 km/s can be evaluated for the portions of isochrones with $\log g \geq 4.0$ or ≤ 3.0 , respectively. For instance, according to Fig. 4, stellar models for $[\text{Fe}/\text{H}] = -0.5$, $[\alpha/\text{Fe}] = 0.2$, $\log g = 4.0$, and $T_{\text{eff}} = 5576$ K will be brighter in *U* and *B* by ≈ 0.04 and ≈ 0.01 mag, respectively, and they will therefore have bluer *U* – *B* colours by ≈ 0.03 mag, if the transformations to *U* and *B* are derived from MARCS models for $v_T = 1.0$ km/s instead of those for $v_T = 2.0$ km/s. The magnitude and colour differences are clearly much smaller at lower metallicities or in the case of redder filters, where the magnitude differences are in the opposite sense. Not unexpectedly, the dependencies of *F336W* and *F438W* magnitudes on v_T are quite similar to those predicted for *U* and *B*. The same can be said of the results for other filters that are located at similar wavelengths, such as *F606W* and *V* or *F814W* and *I_C*. Although not shown, an increase in v_T from 2.0 km/s to 5.0 km/s gives rise to *fainter* *U*, *B*, *F336W*, and *F438W* magnitudes by up to a few tenths of a magnitude, depending on the assumed stellar properties; see e.g., CV14, their Figs. 3 and 4⁴ and the associated discussion.)

Interestingly, the bottom panel of Fig. 4 shows that the recent improvements to MARCS synthetic spectra imply brighter magnitudes at blue and UV wavelengths than those derived from the Gustafsson et al. (2008) spectra. Note that the actual magnitude differences due solely to the improved treatment of the blanketing are less than those shown because the *s21std* and *s08std* BCs assume different microturbulent velocities. This can be corrected by subtracting the predicted magnitude differences in the upper panel from those plotted in the lower panel, resulting in, e.g., $\delta(U) \approx 0.08$ mag and $\delta(F336W) \approx 0.09$ mag at $[\text{Fe}/\text{H}] = -0.5$. In the case of *V*, *F606W*, and redder filters in both photometric systems, the BCs and synthetic magnitudes based on the current MARCS models are nearly identical with those determined from the Gustafsson et al. computations. As shown in § 5 and Paper II, observations appear to provide unambiguous support for the application of systematic corrections to the CV14 BCs such as those implied by the lower panel of Fig. 4 — including the reduction in v_T for dwarf stars.

Histogram plots also provide a good way of visualizing the effects on a spectrum of varying the mixture of the metals. Figure 5 is similar to the previous figure except that the latest BCs

for the standard $[\alpha/\text{Fe}] = 0.4$ mix (i.e., the *a4s21* case) have been subtracted from the BCs that are obtained on the assumption of a number of chemical abundance variations (specifically, *a4CNN*, *a40NN*, etc.), as identified in each panel. This particular plot assumes $\log g = 3.0$, which is characteristic of stars that are located on the lower RGB, and the temperatures derived from 12.5 Gyr isochrones for $[\text{Fe}/\text{H}] = -2.5, -1.5, \text{ and } -0.5$ at this gravity. According to panel (a), enhanced N (and CN) abundances mainly affect the flux at short wavelengths (due to increased strengths of CN bands; see Sbordone et al. 2011.). For instance, lower RGB stars with $[\text{Fe}/\text{H}] = -0.5$ and $[\alpha/\text{Fe}] = 0.4$ are expected to have increased *U* magnitudes by $\delta(U) = -\delta(\text{BC}_U) \approx 0.07$ mag, as compared with $\delta(U) \approx 0.03$ mag for stars with $[\text{Fe}/\text{H}] = -1.5$ at a similar evolutionary state. Since the effects on *B* and *F438W* magnitudes are in the opposite sense, enhanced CN is predicted to cause significantly redder *U* – *B* and $m_{F336W} - m_{F438W}$ colours. Such enhancements apparently have relatively minor consequences for the IR magnitudes of stars that are just beginning their ascent of the RGB.

If most of the C and O are converted to N as the result of ON-cycling, the resultant BCs are qualitatively and quantitatively quite similar to those found for the *a4CNN* case; compare the results in panel (b) with those shown in panel (a). Because the *U* and *F336W* passbands include an NH band, the respective magnitudes are especially dependent on the N abundance. However, they also have some sensitivity to the abundance of oxygen (see panel c), and differences in this dependence are presumably responsible for the variations between panels (a) and (b) of the $\delta(\text{mag})$ values for these two filters. (MARCS synthetic spectra show that OH and NH are prominent in the *F336W* passband, along with CN in the reddest part of it.) Note that, even if oxygen is enhanced by as much as 0.4 dex (panel c), the consequences of such a large enhancement on the UV, optical, and IR magnitudes and colours of lower RGB stars are relatively minor.

A 0.4 dex increase in the abundance of carbon, as illustrated in panel (d), is much more consequential. At $[\text{Fe}/\text{H}] > -1.5$, high C results in fainter *U* and *B* magnitudes by a few to several hundredths of a magnitude (up to ~ 0.12 mag at $[\text{Fe}/\text{H}] \sim -0.5$) along with appreciably redder *U* – *B* and *B* – *V* colours. Interestingly, carbon affects the magnitudes measured by the *F438W* passband more than those derived from shorter or longer wavelength filters, such that, e.g., $m_{F336W} - m_{F438W}$ colours become bluer, while $m_{F438W} - m_{F606W}$ colours become redder, as the result of increased C abundances. Fig. 5d also shows that Mg, which is an important contributor to the opacity in the atmospheric layers of lower RGB stars (see the plots provided by VandenBerg et al. 2012, their Figs. 7–11), is much less important for the BCs of such stars at fixed values of $\log g$ and T_{eff} than C or N. This panel indicates that a 0.2 dex enhancement will affect predicted Johnson-Cousins-2MASS and WFC3 magnitudes at the level of $\lesssim 0.01$ – 0.02 mag.

However, these results cannot be taken at face value because giants with enhanced abundances of Mg (and/or Si) are predicted to be cooler (see, e.g., VandenBerg et al. 2012), which must be taken into account when stellar models are transposed to observational CMDs. Variations in the abundances of C, N, and O are not expected to affect the temperatures of lower giant-branch stars because their electrons are quite tightly bound; i.e., they have high ionization energies. Hence, it is necessary to take into account the impact of the assumed chemical abundance variations on the T_{eff} s of stars when evaluating how such variations alter their CMD locations. Before investigating this aspect of the problem (in the next section), it is worthwhile to consider the gravity dependence of such results as those shown in Fig. 5.

⁴ Note that the $\Delta(\text{mag})$ values plotted in the two figures given by CV14 are in the sense $\text{mag}(v_T = 2) - \text{mag}(v_T = 1)$ (blue points) and $\text{mag}(v_T = 2) - \text{mag}(v_T = 5)$ (red points), which is opposite to the convention adopted in our Fig. 4.

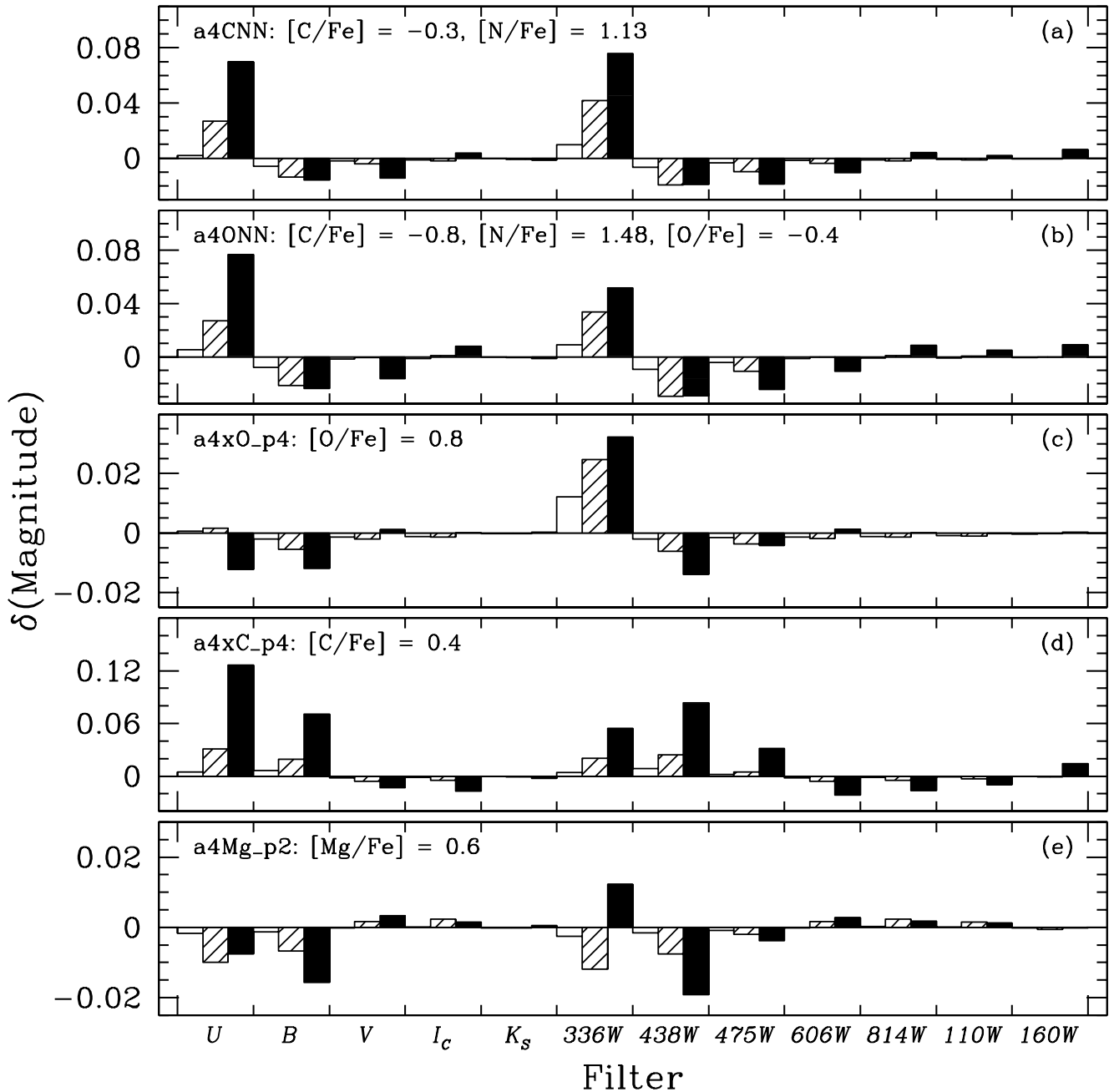


Figure 5. Similar to the previous figure, except that the BCs for the reference a4s21 mix have been subtracted from those for the indicated mixtures. The models assume $\log g = 3.0$ and $T_{\text{eff}} = 5283, 5166,$ and 4831 K, as predicted by 12.5 Gyr isochrones for $[\text{Fe}/\text{H}] = -2.5, -1.5,$ and $-0.5,$ respectively, at the selected gravity. Note that there are differences in the ordinate scales of the various panels.

In the case of (warmer) turnoff stars, which have gravities close to $\log g = 4.0$, the corresponding histogram plot, which is not included here because it is relatively simple and easy to describe in a few sentences, closely resembles Fig. 5, except that the derived $\delta(\text{mag})$ values are much smaller. At $[\text{Fe}/\text{H}] \leq -1.5$, they amount to only a few thousandths of a magnitude; consequently, the magnitudes and colours of the most metal-poor TO stars are not significantly affected by variations in the C:N:O abundance ratio or enhancements in the abundances of C, O, Mg, or Si. At a metallicity as high as $[\text{Fe}/\text{H}] = -0.5$, it is only the synthetic UV magnitudes that are impacted by ≥ 0.02 mag. For instance,

$\delta(U) \approx +0.04, +0.04, -0.0005, +0.03,$ and -0.003 mag for, in turn, the a4CNN, a4ONN, a4x0_p4, a4xC_p4, and a4Mg_p2 cases, with similar findings for $\delta(F336W)$.

More interesting is the histogram plot for $\log g = 5.0$, which is shown in Figure 6. Mixtures of C and N arising from CN-cycling are not expected to affect the broad-band magnitudes and colours of lower main sequence (LMS) stars by more than ~ 0.03 mag (see panel a), though it is curious that $F336W$ magnitudes at the lowest $[\text{Fe}/\text{H}]$ values are fainter by 0.03–0.05 mag when the a4CNN models generally predict somewhat brighter magnitudes in nearly all other passbands. As shown in panels (b) and (c), oxygen has a

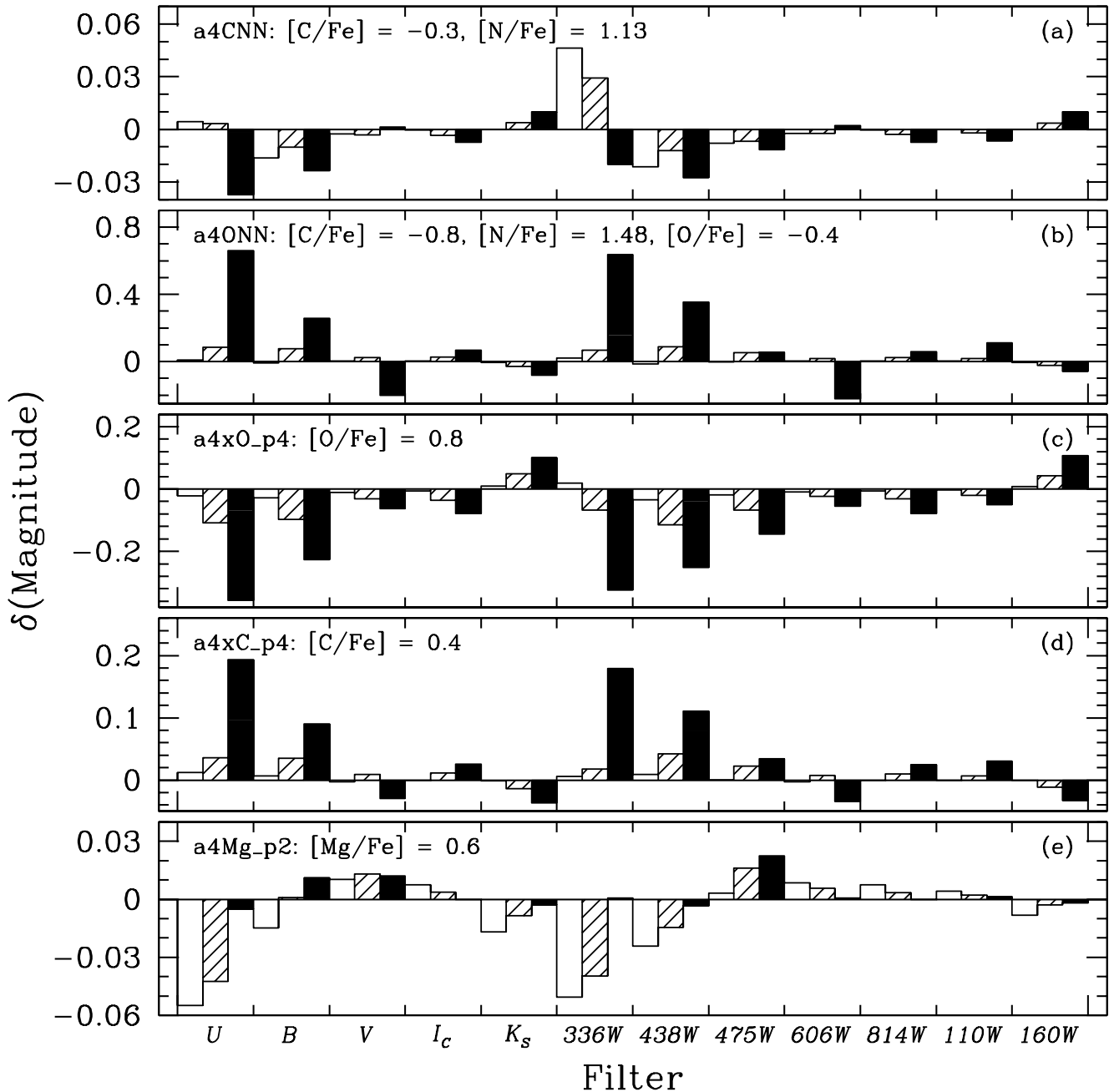


Figure 6. Similar to the previous figure, except that the models assume $\log g = 5.0$ and $T_{\text{eff}} = 4170, 3828$, and 3365 K, as predicted by 12.5 Gyr isochrones for $[\text{Fe}/\text{H}] = -2.5, -1.5$, and -0.5 , respectively, at the selected gravity.

dominating influence on the photometric properties of LMS stars, especially at higher metallicities. However, even at $[\text{Fe}/\text{H}] \sim -1.5$, reduced or enhanced O abundances can affect predicted magnitudes at a given T_{eff} by ~ 0.1 mag; note the very wide range in the ordinate values of panel (b). According to Figs. 6b and 6c, the $\delta(\text{mag})$ values for other than the V and K_S filters (or F606W and F160W in the case of WFC3 photometry) are larger when the O abundance is reduced, and vice versa, or when C is enhanced (panel d). Finally, enhancements in Mg apparently have bigger consequences for predicted magnitudes (at UV and blue wavelengths, in particular) when $[\text{Fe}/\text{H}] = -2.5$ and -1.5 than at $[\text{Fe}/\text{H}] = -0.5$; see panel (e). However, as noted above, the translation of such findings to ob-

served CMDs depends on how the model T_{eff} scale is affected by the assumed metal abundance variations. An investigation of this issue is the next step in our analysis.

4 ISOCHRONES FOR DIFFERENT MIXTURES OF THE METALS

The version of the Victoria stellar evolution code that has been documented in considerable detail by Vandenberg et al. (2012, and references therein) has been used to compute all of the evolutionary tracks that were needed for this project. The basic physics

and the careful treatment of the gravitational settling of helium incorporated in it can be regarded as state-of-the-art. As shown by VandenBerg et al. (2016), the tracks produced by the Victoria code are essentially indistinguishable from those derived from the MESA code (Paxton et al. 2011) when as close as possible to the same physics is adopted. The diffusion of the metals is not considered, but this is largely inconsequential for the predicted T_{eff} scale, when extra mixing below surface convection zones is treated, and for turnoff luminosity versus age relations (see the discussion by VandenBerg et al. 2014). In fact, isochrones that are generated from Victoria tracks, using software described by VandenBerg et al. (2012, and references therein), match the observed MS and RGB slopes in GC CMDs, as well as their morphologies in the vicinity of the TO, exceedingly well (see, e.g., VBLC13). Several studies have also demonstrated that Victoria computations do a good job of satisfying the constraints provided by solar neighborhood stars with well-determined distances (VandenBerg et al. 2010), the RR Lyrae standard candle e.g., VandenBerg et al. 2016, Denissenkov et al. 2017), and binary stars in open clusters (Brogaard et al. 2012) and GCs (Brogaard et al. 2017, VandenBerg & Denissenkov 2018).

Moderately large grids of stellar models have already been published by VandenBerg et al. (2014) for $[\alpha/\text{Fe}] = -0.4, 0.0, +0.4$, and the standard variation of $[\alpha/\text{Fe}]$ with $[\text{Fe}/\text{H}]$, assuming in each case wide ranges in $[\text{Fe}/\text{H}]$ and Y . The isochrones derived from them, which are generally referred to as the “Victoria-Regina isochrones”, adopted the solar abundances given by Asplund et al. (2009) as the reference mixture of heavy elements. Indeed, as discussed in § 2.1, we have opted to make the same assumption here in order that the corresponding evolutionary computations are part of the same family as the 2014 computations.

As in the previous investigation, opacities for each of the assumed mixtures of the metals were obtained from the OPAL website⁵ (see Iglesias & Rogers 1996, and references therein) for temperatures $\gtrsim 10^4$ K, while they were generated using the codes described by Ferguson et al. (2005) for lower temperatures. Since we are interested in the predicted temperatures, as well as the colours, of models for different mixtures of the metals, it is worth mentioning that the properties at $\tau = 100$ of MARCS model atmospheres for the different chemical abundance choices were used to define the boundary conditions of our stellar interior models at relatively high gravities (masses $\lesssim 0.4M_{\odot}$). At higher masses, it is preferable, for reasons given by VandenBerg et al. (2014), to derive the boundary pressure by integrating the hydrostatic equation from small optical depths to the photosphere in conjunction with a $T-\tau$ relation based on an empirical solar atmosphere or accurate 3D models for the atmosphere of the Sun; see Pereira et al. (2013). Our stellar models employed the $T-\tau$ relation derived by VandenBerg & Poll (1989) to represent the Holweger & Mueller (1974) solar atmosphere. Those wanting more details concerning the Victoria code and/or the methods used to generate evolutionary tracks and isochrones are encouraged to refer to the VandenBerg et al. (2012, 2014) studies.

4.1 Comparisons of Isochrones on the H–R Diagram

Figure 7 illustrates the upper MS, TO, and lower red-giant branches of 12.5 Gyr isochrones for $[\text{Fe}/\text{H}] = -2.5, -1.5$, and -0.5 and the indicated mixtures of the metals. At the lowest metallicity, the isochrones are nearly coincident except in the vicinity of the TO and subgiant branch (SGB) for those cases having higher $[\text{CNO}/\text{Fe}]$

than the a4s21 mix; higher C+N+O results in a fainter TO and SGB at a given age, and vice versa (see, e.g., VandenBerg et al. 2012). In general, the temperatures of MS or RGB stars are not affected by variations in either the ratio C:N:O or the total C+N+O abundance. Furthermore, it is only at higher $[\text{Fe}/\text{H}]$ values where the effects of increased Mg and Si abundances become evident (see the loci labelled a4Mg_p2 and a4Si_p2) — not just near the TO, but also along the RGB. As shown by VandenBerg et al., Mg and Si have quite a strong influence on the predicted temperatures of giants because they are two of most abundant metals that are also important electron donors (unlike, e.g., O and Ne).

It should be appreciated that Mg abundance variations associated with the observed Mg–Al anticorrelations in some GCs is a separate issue. If $\text{Mg}+\text{Al} = \text{constant}$, which seems to be typical of the majority of GCs (see Carretta et al. 2009b), Mg–Al anticorrelations have no significant ramifications for isochrones (Salaris et al. 2006, Pietrinferni et al. 2009). In fact, it has been discovered that $[\text{Si}/\text{Fe}]$ is correlated with $[\text{Al}/\text{Fe}]$ when the abundance of Mg is reduced by a large amount, which indicates that there is leakage into ^{28}Si from the Mg–Al cycle (Yong et al. 2005, Carretta et al. 2012, Carretta et al. 2018). In the case of NGC 4833, for instance, Carretta et al. (2014) have found that a 0.5 dex reduction in the Mg abundance is accompanied by increased abundances of Al and Si by about 1 dex and 0.2 dex, respectively, which is close to the expected abundances if $\text{Mg}+\text{Al}+\text{Si} = \text{constant}$. Indeed, if this condition is satisfied, isochrones that allow for different abundances of Mg, Al, and Si will be nearly identical with those computed for the standard mix (see Cassisi et al. 2013) given that the effects of higher Al and Si abundances on low-temperature opacities will mostly compensate for those arising from the reduced abundances of Mg. (There should be some differences in the opacity when Mg is converted to Al and Si because Al, in particular, has relatively few atomic lines, but they are likely too small to have significant effects on predicted T_{eff} s at low $[\text{Fe}/\text{H}]$ values.)

Perhaps the most striking result in Fig. 7 is that a higher He abundance by $\delta Y = 0.05$ has larger consequences for the temperatures of MS and RGB stars at a fixed luminosity than nearly all of the metal abundance variations that we have considered. Only 0.2 dex enhancements of Mg and Si at only the highest metallicities, $[\text{Fe}/\text{H}] \gtrsim -0.5$, have comparable effects on the predicted temperatures along the giant branch. The models for higher Y , which have been given the name a4_dY05, were taken from the study by VandenBerg et al. (2014), as they were generated for the same relative abundances of the metals as in the a4s21 mix, using exactly the same version of the Victoria stellar evolution code that has been employed in this study. (They are not explicitly listed in Table 1 because BCs were not calculated specifically for this case. As already mentioned, BCs have a very weak dependence on the assumed He abundance; consequently, the same BCs can be safely adopted for both the a4s21 and a4_dY05 chemical abundance mixtures.) Worth noting is the prediction that, at a given age, differences in Y affect the slope of the SGB portion of an isochrone, but not its mean luminosity, which depends primarily on $[\text{CNO}/\text{Fe}]$.

At low masses along the MS ($M/M_{\odot} \lesssim 0.4$), where the blanketing of stars is strongly affected by molecules, the predicted T_{eff} scale depends much more on the mixture of heavy elements than along the upper MS; see Figure 8. Furthermore, C and O clearly affect the temperatures of LMS stellar models more than He if they are more metal rich than $[\text{Fe}/\text{H}] \sim -1.5$. Recall that the properties of fully consistent MARCS model atmospheres at $\tau = 100$ were used to determine the outer boundary conditions of the stellar interior models (notably at $\log L/L_{\odot} \lesssim -1.3$); consequently, the various

⁵ <http://opalopacity.llnl.gov>

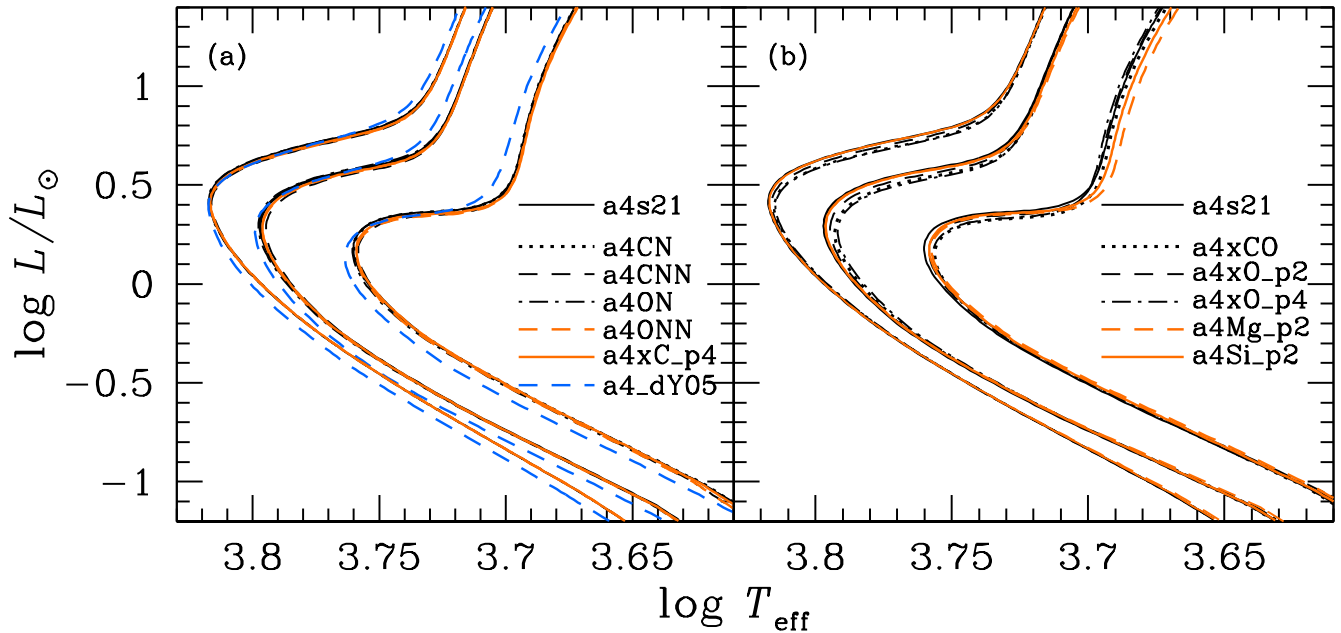


Figure 7. Comparisons of 12.5 Gyr isochrones for the indicated mixtures of the metals (see Table 1) and $[\text{Fe}/\text{H}] = -2.5, -1.5,$ and -0.5 (the three groups of loci in the direction from left to right, respectively). Isochrones for the standard $[\alpha/\text{Fe}] = 0.4$ mix (a4s21), but with higher Y by 0.05 were taken from the study by Vandenberg et al. (2014), and given the name a4_dY05.

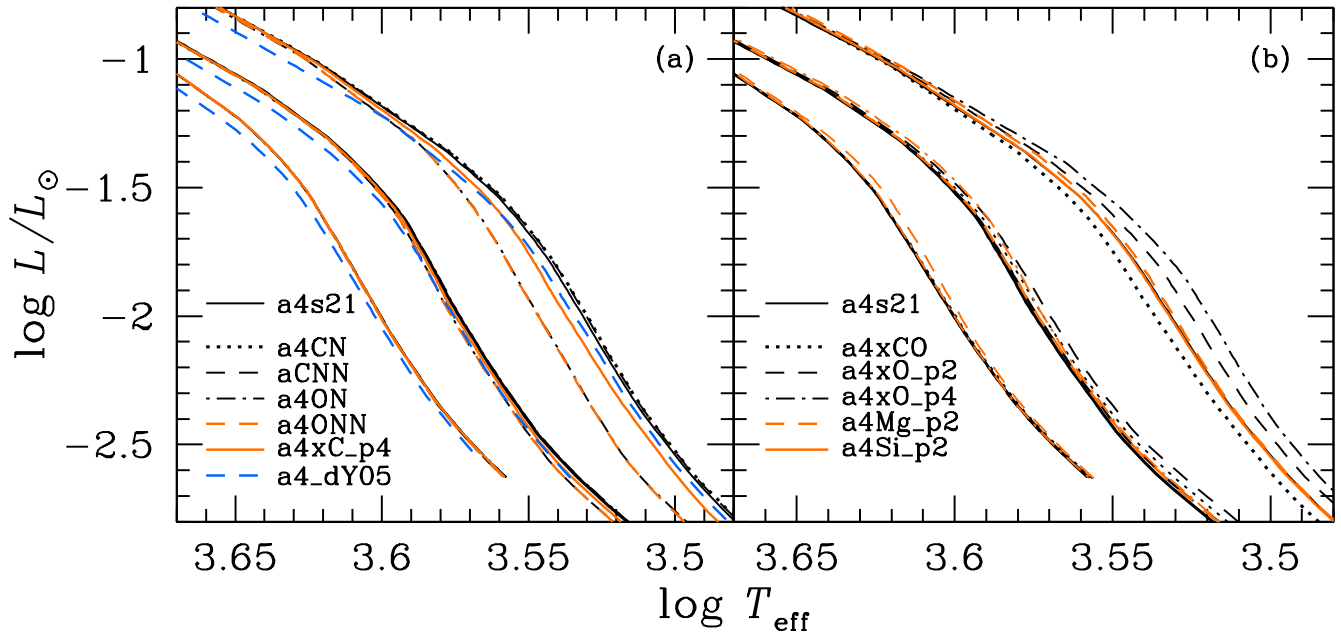


Figure 8. Comparisons of the lower MS portions of the same isochrones that were plotted in the previous figure.

loci represent the best predictions that we are able to make at the present time of both the absolute and relative locations on the H-R diagram of LMS models for different chemical compositions.

Not surprisingly, zero-age main-sequences (ZAMSs) are particularly sensitive to the abundance of oxygen, and somewhat less so to the abundance of carbon. As shown in panel (a), the large reductions in the O abundance that are assumed in the a4ON and a4ONN mixtures shift the respective ZAMS loci to warmer temperatures. Interestingly, these sequences overlay one another almost

exactly, which suggests that the LMS is not very dependent on the abundance of nitrogen since the only difference between these two cases is that the a4ON models assume a lower N abundance by 0.18 dex than those for the a4ONN mixture (see Table 1). In view of these results, one can anticipate that significantly higher O abundances will result in cooler LMS models, which is borne out by our computations for the a4x0_p2 and a4x0_p4 mixtures; see panel (b). Carbon appears to affect LMS models in the opposite sense; i.e., low-mass stars with enhanced C abundances are predicted to

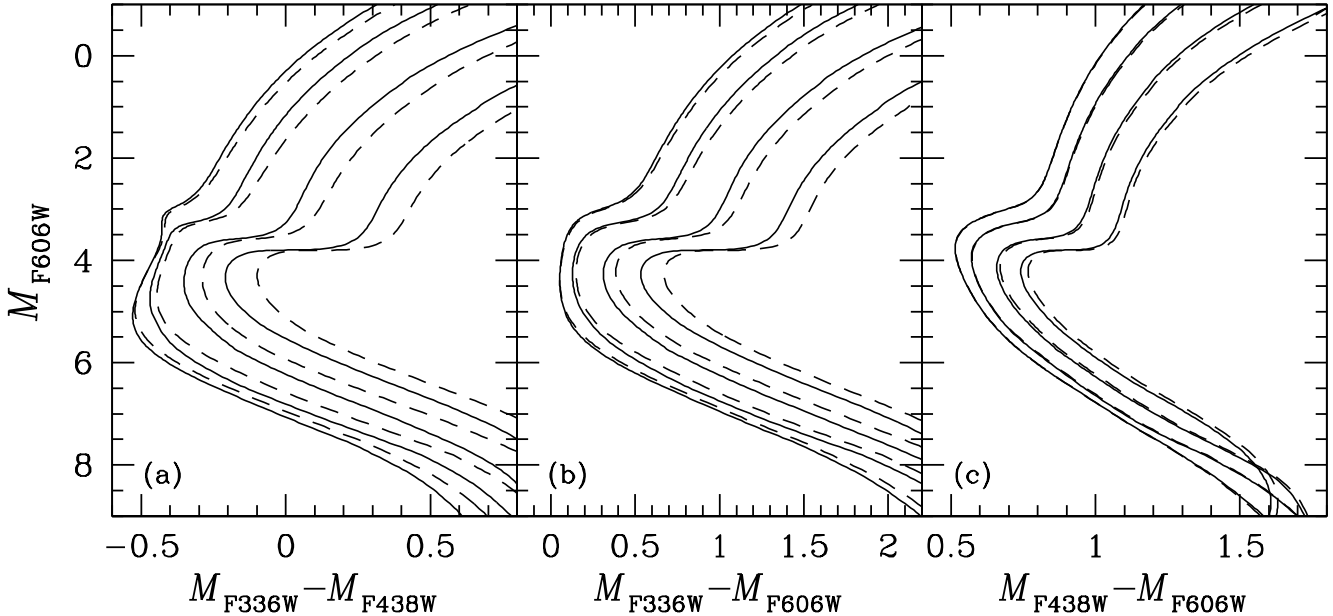


Figure 9. Comparison of 12.5 Gyr isochrones for $[\alpha/\text{Fe}] = 0.4$ and $[\text{Fe}/\text{H}] = -2.0, -1.5, -1.0,$ and -0.5 that have been transformed to three CMDs involving WFC3 filters using the BCs reported by CV14 (dashed curves) and the BCs calculated for this study (solid curves). In the case of the $M_{F606W} - M_{F814W}$ colour index (not shown), the differences between the solid and dashed loci are less than half of those shown in the right-hand panel for $M_{F438W} - M_{F606W}$ at the same metallicities.

be warmer —see our results for the a4xC_p4 and a4xC0 mixtures. The ZAMS for the latter case differs only slightly from the former, even though it assumes a higher value of $[\text{C}/\text{Fe}]$ by 0.3 dex, probably because of the compensating effects of also assuming a higher O abundance by 0.2 dex, which would tend to displace LMS stars to cooler temperatures.

As shown in Figure 8, the temperatures of low-mass ZAMS models for $[\text{Fe}/\text{H}] \leq -0.5$ are unaffected by variations in the abundance of Si or C:N abundance ratios. The bottom of the MS has some sensitivity to the abundance of Mg, but the effects of variations in the abundances of C, O, and He are much more important. The a4CNN case, which is similar to a4CN but with a higher N abundance, resulting in higher C+N+O (see Table 1, is predicted to be cooler than the others, but only marginally, even at the highest $[\text{Fe}/\text{H}]$ value. These findings confirm the conclusions reached by Pietrinferni et al. (2009), from their own computations of stellar models, that standard α -element enhanced isochrones can be used to represent the CN-weak and CN-strong sub-populations in GCs. Although these sub-populations may be separated photometrically through the use of suitable filters, that separation is entirely a bolometric corrections effect, not an indicator of differences in T_{eff} . Of course, this has long been known from spectroscopic work, such as that by Cannon et al. (1998) who found that CN-weak and CN-strong stars in 47 Tuc overlay one another on the $(B-V)$, V -diagram from the upper giant branch to below the MS turnoff with no discernible differences in their CMD locations.

Most of the results reported in this section confirm the conclusions reached in earlier studies (several of which are referenced in § 1). The advantages of our investigation are that (i) unlike nearly all published work on this subject to date, our models for different abundance variations have been computed at constant $[\text{Fe}/\text{H}]$, rather than at constant Z (the mass-fraction abundance of all elements heavier than helium), to facilitate quantitative comparisons with observations, and (ii) our findings are based on fully consis-

tent, up-to-date atmosphere-interior models, which should result in improved quantitative predictions of the dependence of the BCs on chemical abundances.

4.2 Comparisons of Isochrones on Selected WFC3 CMDs

Before intercomparing the isochrones for different mixtures of the metals on various CMDs, a brief examination of the observational consequences of the BCs that have been generated for this project and those calculated by CV14 from the synthetic fluxes published by Gustafsson et al. (2008) is warranted. Plotted in Figure 9 are 12.5 Gyr isochrones for $[\alpha/\text{Fe}] = 0.4$ and $[\text{Fe}/\text{H}] = -2.0, -1.5, -1.0,$ and -0.5 , as transformed to three different CMDs using the CV14 BCs (dashed curves) and the updated BCs presented here (solid curves). This shows that the differences in the BCs (see the histogram plots in § 3) result in systematically bluer colours at shorter wavelengths, by as much as ~ 0.12 mag in colours that involve M_{F336W} , but by $\lesssim 0.015$ mag in the case of optical colours. Due to the increasing complexity of spectra towards shorter wavelengths, improvements to the treatment of atomic lines and molecular bands are bound to have the biggest impact on BCs in the UV.

The next three figures illustrate the main results of this investigation. As discussed by Piotto et al. (2015), the $F336W$ and $F438W$ filters provide the means to discriminate between stars with different CN strengths. To be more specific: because the $F336W$ passband contains an NH band, N-rich stars will have fainter $F336W$ magnitudes than those described as CN-weak stars. Similarly, given that the $F438W$ passband includes CN and CH bands, C-rich stars will be fainter in $F438W$; consequently, stars containing CNO-processed material will have redder $m_{F336W} - m_{F438W}$ colours than those with $[\text{C}/\text{Fe}]$ and $[\text{N}/\text{Fe}] \sim 0$. These expectations are confirmed by the BC histogram plots in our Fig. 5, as well as the upper left-hand panel in Figure 10, which shows that that the a4CN and a4CNN isochrones, with reduced C and enhanced

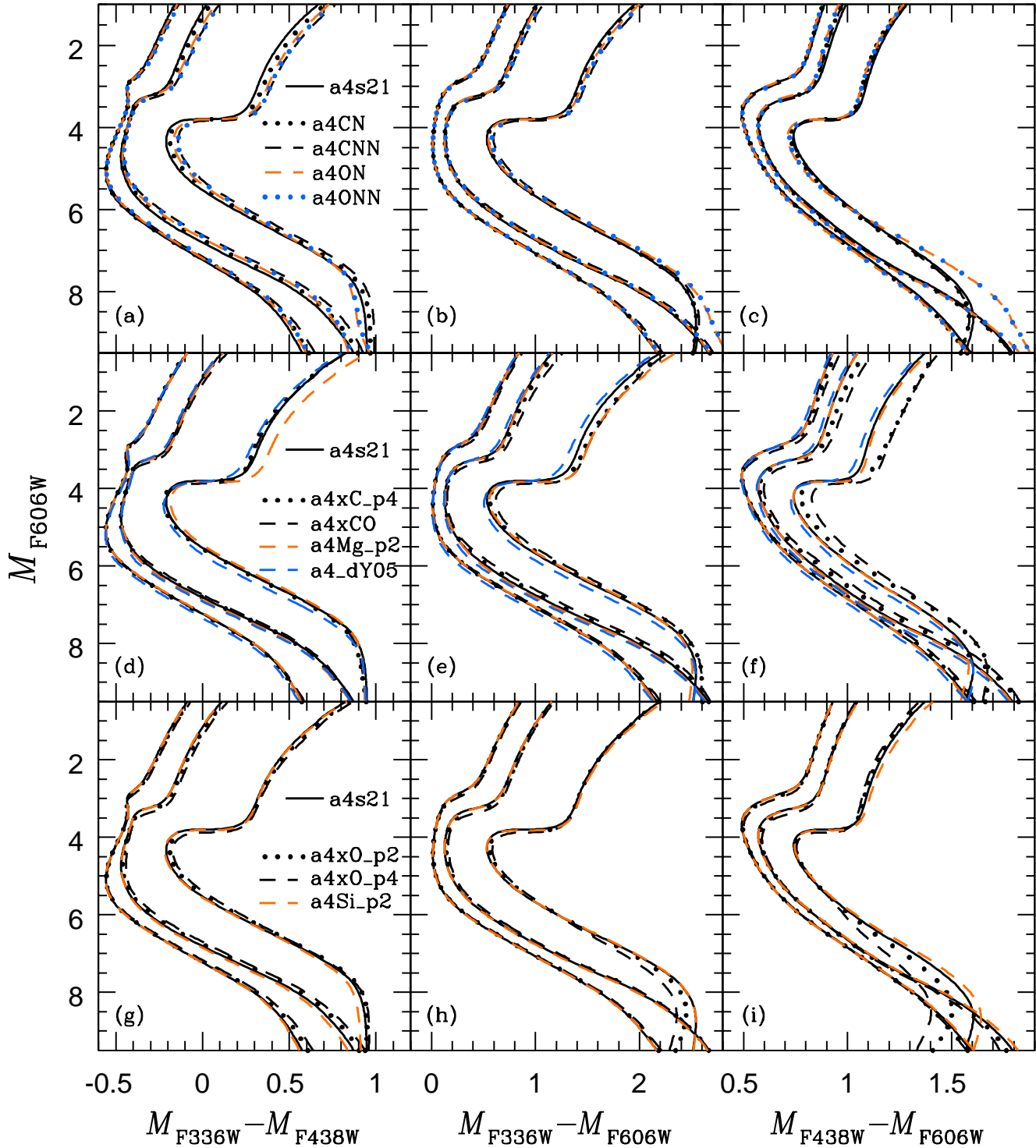


Figure 10. Comparisons of 12.5 Gyr isochrones for $[\alpha/\text{Fe}] = +0.4$ and $[\text{Fe}/\text{H}] = -2.5, -1.5,$ and -0.5 , assuming the mixtures of the metals that are specified in the left-hand panels. Isochrones for higher Y (the $a4_dY05$ loci) were transposed to the observed planes using the $a4s21$ BCs given that bolometric corrections have very little sensitivity to the adopted He abundance.

N abundances, are significantly redder than those for scaled-solar abundances of C and N (the solid curve representing the $a4s21$ mixture) on the $M_{F336W} - M_{F438W}$, M_{F606W} diagram. Note that the isochrones for the $a4ON$ and $a4ONN$ mixtures, which assume somewhat higher N abundances, are displaced to even redder colours along the MS and RGB, though bluer colours are predicted for

these cases along the LMS (because low-mass stars with depleted O abundances are predicted to be considerably warmer than those with normal abundances ($[\text{O}/\text{Fe}] \sim 0.4$); see Fig. 8).

Variations in the C, N, and O abundances due to CN- and ON-cycling have much smaller consequences for the colours of MS and lower RGB stars that are derived from the $F438W$, $F614W$,

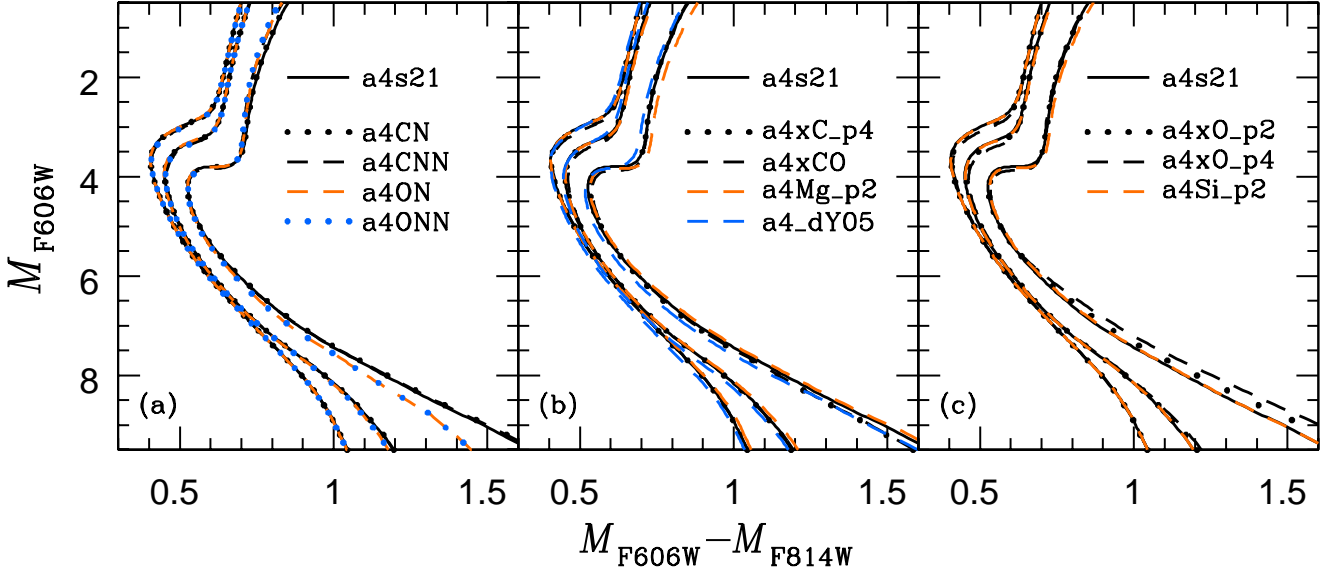


Figure 11. As in the previous figure, except that the isochrones are compared on the $M_{F606W} - M_{F814W}$, M_{F606W} diagram.

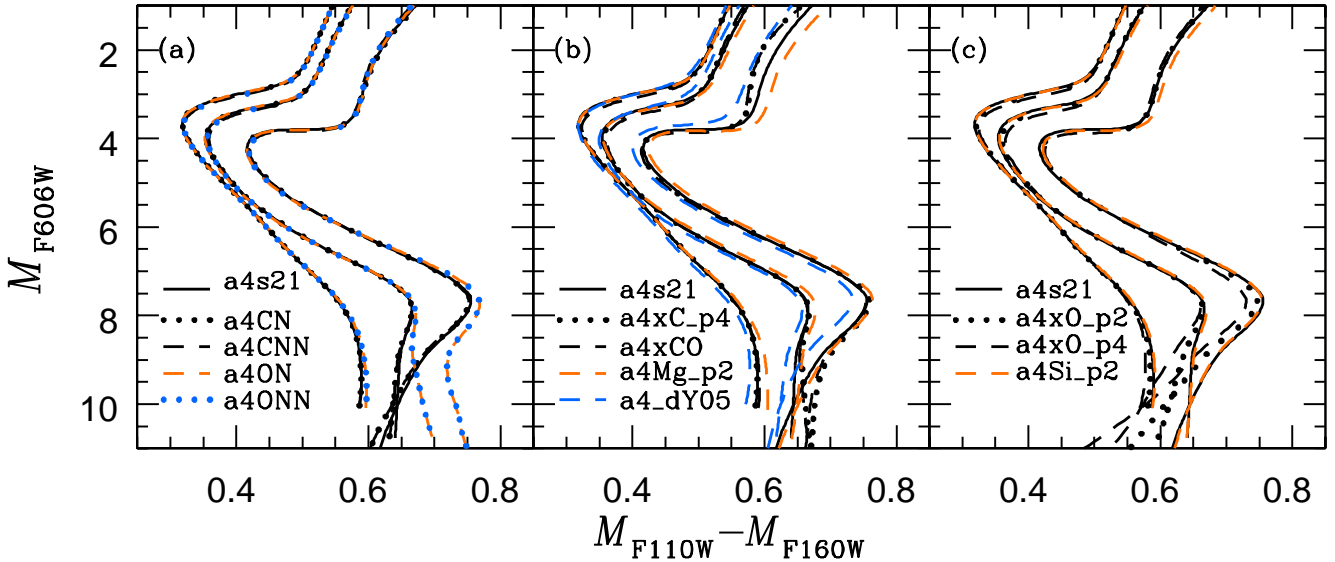


Figure 12. Comparisons of the predicted IR colours along 12.5 Gyr isochrones for $[\text{Fe}/\text{H}] = -2.5, -1.5,$ and -0.5 with the indicated mixtures of the metals.

and $F814W$ passbands. Such colours, as shown by the isochrones plotted in Fig. 10c and the left-hand panel of Figure 11, tend to be somewhat bluer, which is a direct consequence of differences in the respective BCs (see, e.g., Fig. 5) Although Fig. 10b suggests that $M_{F336W} - M_{F606W}$ is less sensitive to N abundances than $M_{F336W} - M_{F438W}$, this impression is due entirely to the fact that the abscissa scale of the middle panel is compressed by a factor of two compared with that adopted for the left-hand panel.

The large CMD-to-CMD variations in the location of the LMS models for the a4ON and a4ONN mixtures relative to those for the standard mix (a4s21) reflect the very different T_{eff} dependencies of the BCs for the WFC3 filters at high gravities. For instance, at $\log g \gtrsim 4.7$, the $\delta(\text{BC})$ values plotted in Fig. 2 for the a4ON mixture (also assuming $[\text{Fe}/\text{H}] = -0.5$), vary strongly with temperature, which results in apparently very steep functions of gravity. Interpo-

lations in those data yield $\delta(\text{BC})$ values of $+0.01, -0.13, +0.13,$ and -0.02 mag for, in turn, the $F336W, F438W, F606W,$ and $F814W$ filters at $\log g = 4.85$. If the corresponding $\delta(\text{colour})$ values are calculated, one obtains the predicted offsets of the ZAMS loci at $M_{F606W} \sim 9.4$ that have been plotted in the top row of panels in Fig. 10 and the left-hand panel of Fig. 11. Since the spline fits to the $\delta(\text{BC})$ values in Fig. 2 must necessarily pass through the predictions for $\log g = 4.7$ and 5.0 , the interpolations for intermediate gravities should be quite trustworthy. In any case, comparisons with observations, such as those presented in Paper II, must be carried out to validate the models.

As expected, enhanced C abundances have the largest effects on $M_{F336W} - M_{F438W}$ colours, making them considerably redder than those predicted for scaled-solar abundances (see Fig. 10f). In the case of lower RGB stars, the separation of the a4xC_p4 models

from those for the a4s21 mix, as well as the prediction that higher C causes somewhat bluer $M_{F336W} - M_{F438W}$ colours, follows directly from the dependence of the BCs on the C abundance (see Fig. 5) — since enhanced carbon has almost no impact on the temperatures of evolved stellar models, as shown in Fig. 7. The middle row of panels in Fig. 10, along with Fig. 11b, also highlight the importance of Mg, especially at higher metallicities, and He. For both of these elements, the shifts in the colours of the respective isochrones are mostly a reflection of temperature offsets relative to the a4s21 isochrone rather than to variations in the BCs due to increased abundances. At fixed values of T_{eff} , a 0.2 dex enhancement in the abundance of Mg affects the BCs at the level of only $\sim 0.005\text{--}0.015$ mag (see Fig. 5).

The bottom row of plots in Figure 10 and Fig. 11c show how the CMD locations of isochrones for the same age and metal abundances are affected by altering the abundance of oxygen and silicon, the former by 0.2 and 0.4 dex and the latter by 0.2 dex. Consistent with the implications from BC calculations (such as those in Fig. 5), our models indicate that upper MS, TO, and lower RGB stars are affected by O abundance enhancements in only a relatively minor way — except at higher metallicities (see panel i). $F606W$ is probably the filter that is most sensitive to the presence of TiO bands, which will be especially prominent in spectra of cool, metal-rich stars. Moreover, a significant gravity dependence is expected because both the Ti and O pressures, and hence the TiO pressure, are sensitive to the overall gas pressure, and therefore $\log g$. In the case of LMS stars, in which many other molecules involving O form (notably H_2O), both the predicted T_{eff} s (Fig. 8) and the BCs (Fig. 6) are very dependent on the abundance of oxygen, though not always in the same sense. That is, even though stellar models that allow for O abundance enhancements are cooler than those without such enhancements, it is not necessarily the case that they are also redder. In fact, as shown in Fig. 10i, $M_{F438W} - M_{F606W}$ colours are bluer, whereas $M_{F606W} - M_{F814W}$ colours (see Fig. 11c) are redder if O has increased abundances.

We conclude this section with an intercomparison and brief discussion of the predicted $M_{F110W} - M_{F160W}$ colours of stellar models. Plotted in Figure 12 are isochrones for the same ages, metallicities, and the various chemical abundance mixtures, as indicated, that were the subject of the two previous figures. The effects on the colours of varying the abundances of He, C, O, Mg, and Si, as well as the ratio C:N:O and [CNO/Fe], are all clearly displayed. MS and RGB stars with enhanced Mg and Si are cooler along the giant branch, resulting in redder IR colors, particularly at higher metallicities, while the reverse is true if they have higher Y . As expected from the relevant BCs in Fig. 5, giants with increased C abundances are predicted to have bluer $M_{F110W} - M_{F160W}$ colours. However, oxygen clearly plays a major role in determining the colours of LMS stars in the IR, as already pointed out by Milone et al. (2019) in their study of NGC6752. If the LMS stars in GCs span a wide range in the $m_{F110W} - m_{F160}$ colour at a given magnitude, the bluest ones are likely to have oxygen abundances that are close to initial abundances (i.e., when they formed), while the reddest ones are likely to be members of the cluster’s most oxygen-poor population, though they could also be C-rich stars; see Fig. 12b.

5 NGC 6496: AN INITIAL TEST CASE

Since the effects of metal abundance variations on the colours of stars become larger with increasing [Fe/H], mainly because (i) there

are more atoms of the metals at higher metallicities and (ii) more metal-rich stars at a similar evolutionary state are cooler, one might expect that WFC3 observations of the most-metal rich GCs will present the greatest challenge for stellar models. Indeed, to obtain a first impression of the capabilities of our improved BCs over those given by CV14, which are based on the previous generation of MARCS model atmospheres and synthetic spectra, we decided to fit isochrones to observations of NGC 6496. According to Carretta et al. (2009a), this cluster has [Fe/H] = -0.46 , making it one of the best available targets for the fitting of the highest metallicity ([Fe/H] = -0.5) isochrones that have been computed for mixtures of the metals in the “a4” series.

WFC3 photometry reported by Nardiello et al. (2018) was obtained via the website that they provide. The CMD was limited to stars with membership probabilities $\geq 98\%$, photometric errors < 0.02 mag, and quality-of-fit (QFIT) parameters ≥ 0.99 . Because we are primarily interested in the upper MS, TO, and lower RGB stars, we opted to use their so-called “Method 1” photometry. The MS and TO observations were sorted into 0.1 mag bins in m_{F606W} , and median fiducial points were determined for each bin. Fitting isochrones to median fiducial sequences has the important advantage that subjective errors have little or no impact on determinations of the best estimate of the cluster age that corresponds to an adopted distance modulus.

Figures 13 and 14 show that isochrones for [Fe/H] = -0.5 , $[\alpha/\text{Fe}] = 0.4$, $Y = 0.26$, and an age of 11.0 Gyr provide a far superior fit to the photometry of NGC 6496, particularly the UV observations, when they are transformed to the various CMDs using the improved BCs (the black loci) rather than those given by CV14 (the orange curve). These plots assume $E(B - V) = 0.235$, which is the line-of-sight reddening according to the Schlegel et al. (1998) dust maps. Indeed, $E(B - V) = 0.22\text{--}0.24$ has also been found in several previous spectroscopic and photometric studies (e.g., Friel & Geisler 1991, Pulone et al. 2003, Abbas et al. 2015, VBLC13). The adopted apparent distance modulus is supported by the fit of a zero-age horizontal branch (ZAHB) locus to the observed HB stars (see VBLC13), and there is ample evidence that distance moduli which are derived in this way are in excellent agreement with empirical distance determinations based on the RR Lyrae and local subdwarf standard candles (see e.g., VandenBerg et al. 2014, VandenBerg & Denissenkov 2018). Assuming that there has been some enrichment of helium since the Big Bang, it is reasonable to adopt $Y = 0.26$ for NGC 6496. Whether or not a somewhat lower or higher value of Y is more appropriate for this GC is, anyway, a moot point because small changes to the assumed He abundance will have only minor consequences for the fits to the photometric data.

Both of the solid curves assume the a4s21 metal abundance mixture, while the dashed isochrone assumes the a4CN mix. On the assumption that NGC 6496 has comparable numbers of CN-weak and CN-strong stars, the isochrones have been adjusted horizontally in color by the indicated δX values so that the black loci straddle the median fiducial sequences. Approximately 20% of the differences along the MS between the solid curves in black and orange are due to the reduction in the micro-turbulent velocity from 2 km sec^{-1} , as assumed in the CV14 transformations, to 1 km sec^{-1} , which is the preferred value for dwarf stars in both previous and current MARCS models. As our main purpose in considering NGC 6496 was to check how well our models are able to reproduce observed CMDs, it is very gratifying to find that the colour offsets between theory and observations are small, certainly within the uncertainties associated with the cluster properties (metallicity,

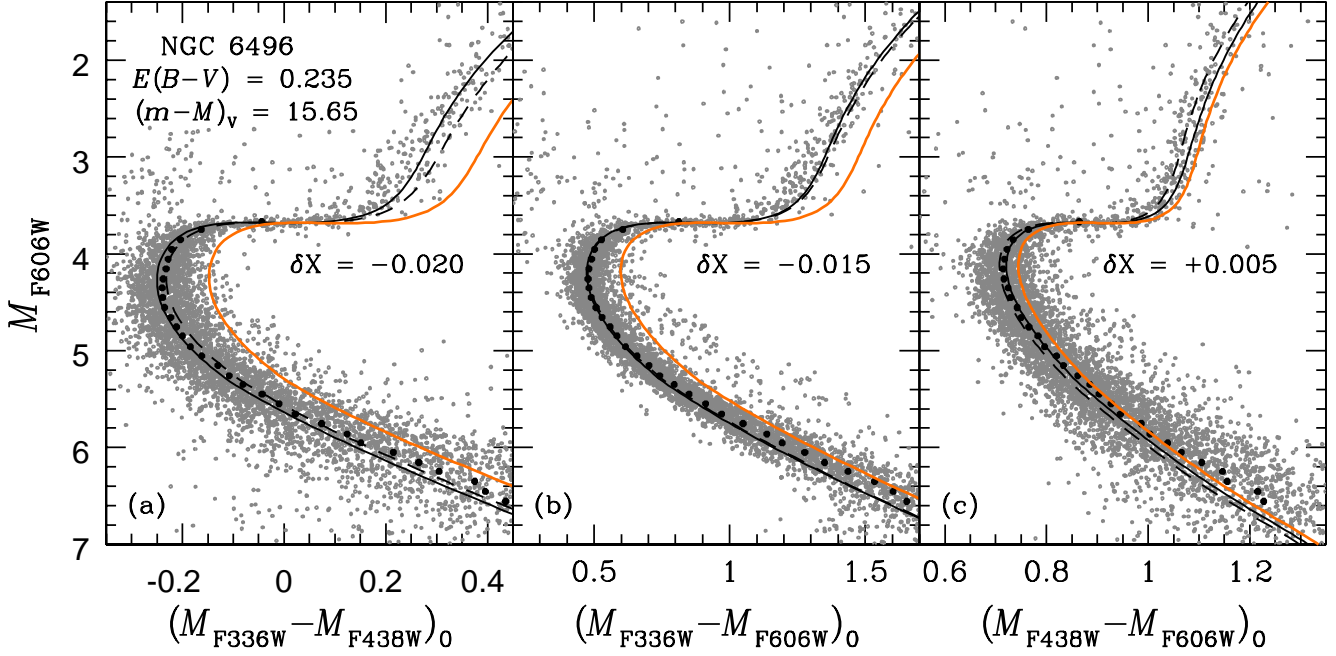


Figure 13. Fits of 11.0 Gyr isochrones for $[\text{Fe}/\text{H}] = -0.5$, $Y = 0.26$, and $[\alpha/\text{Fe}] = 0.4$ to WFC3 observations of NGC 6496 (from Nardiello et al. 2018) on the assumption of the indicated reddening and apparent distance modulus. Isochrones for the a4s21 and a4CN mixtures, using the BCs that were computed for this project, are represented by the solid and dashed loci, in black, respectively. If the CV14 BCs are used instead to transform the a4s21 isochrone to the observed planes, one obtains the solid, orange curves. The isochrone colours were adjusted by the amounts given by the δX values in each panel; these adjustments are needed to obtain satisfactory fits of the black isochrones to the cluster fiducial sequences (filled circles) in the vicinity of the turnoff. Note that, for any colour index $\zeta - \eta$, the colour excess can be calculated from $E(\zeta - \eta) = (R_\zeta - R_\eta)E(B - V)$, using the tabulated values of R_ζ and R_η reported by CV14 (see their Table A1). Information given in the same source provides the means to convert $(m - M)_V$ to $(m - M)_{F606W}$.

reddening), the model T_{eff} scale, and the zero-points of both the photometry and the computed BCs. The relatively large scatter in the colours of turnoff stars is presumably due mostly to photometric errors, with some contributions due to the presence of binaries, perhaps modest star-to-star He abundance variations, and possibly some amount of differential reddening. As discussed in § 3, variations in C:N:O, at constant C+N+O, are predicted to have very little effects on TO colours.

One unexpected result of fitting isochrones to WFC3 observations of NGC 6496 is that the predicted and observed $M_{F606W} - M_{F814W}$ colour of the TO are in excellent agreement, as indicated by the small value of δX in Fig. 14. This is surprising because VBLC13 found that the same Victoria-Regina isochrones, when compared with *HST* Advanced Camera for Surveys (ACS) data for this and ~ 50 other GCs (as obtained by Sarajedini et al. 2007), generally required a blueward shift of ≈ 0.02 mag to reproduce observed turnoffs, independently of the cluster under consideration. Although the $F606W$ and $F814W$ filters in the ACS and WFC3 instruments are not identical, ACS $M_{F606W} - M_{F814W}$ colours for MS stars appear to be just slightly bluer, by ≈ 0.003 mag, than the corresponding WFC3 colours, based on our examination of the CV14 BCs. However, similar comparisons of observed ACS and WFC3 CMDs for the same GC (from Sarajedini et al. 2007 and NLP18, respectively), reveal differences amounting to ≈ 0.018 mag, but in the opposite sense. Clearly, there is a net zero-point difference of about 0.02 mag between predicted and observed $M_{F606W} - M_{F814W}$ colours in the ACS and WFC3 systems. Regardless of whether this is a problem with the BC transformations or with the photometric zero-points, very little, if any, offsets to WFC3 $M_{F606W} - M_{F814W}$ colours for the MS stars in GCs appear to be necessary.

As far as we are aware, Martins et al. (2017) were the first researchers to fit isochrones to UV-optical CMDs derived from WFC3 observations of GCs (specifically NGC6752). Using BCs based on Kurucz ATLAS12 model atmospheres (Kurucz 2014) and synthetic spectra produced by the SYNTH code (Kurucz 2005), they found that their models reproduced the observed $F606W, F814W$ photometry of turnoff stars quite well, but that they are too red along the giant branch — which is qualitatively similar to our results for NGC 6496 (see Fig. 14), as well as the fits to ACS $F606W, F814W$ photometry (Sarajedini et al. 2007) reported by VBLC13 for a few dozen GCs. (The cause of this ~ 0.03 – 0.04 mag discrepancy along the lower RGB is not known at the present time, though we will revisit this problem in Paper II.) Interestingly, Martins et al. found that the predicted $M_{F336W} - M_{F814W}$ colours are too blue for both TO and RGB stars by quite large amounts (~ 0.12 – 0.15 mag, depending on the assumed value of Y). Apparently Kurucz models predict too much flux at short wavelengths, whereas our improved MARCS models, even in the case of clusters that are more metal rich by ~ 1 dex, are not obviously deficient in this regard (see Fig. 13).

The encouraging results that we have obtained for NGC 6496 gives us considerable optimism that our models will fare quite well in applications to other systems which have been much more thoroughly studied insofar as their chemical properties are concerned. In Paper II, we analyze the CMDs derived from WFC3 observations of six GCs (47 Tucanae, NGC 6362, M 5, M 3, M 55, and M 92) that span a range in $[\text{Fe}/\text{H}]$ from ~ -0.7 to ~ -2.4 .

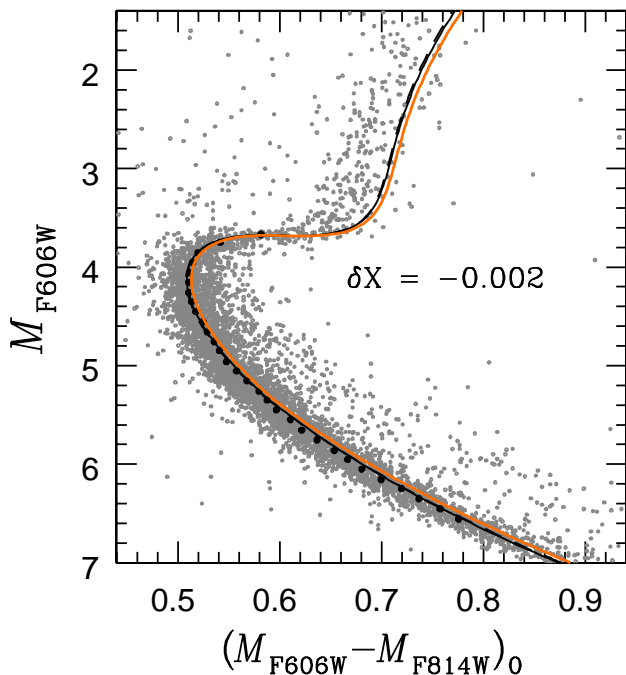


Figure 14. As in the previous figure, except that the isochrones are fitted to $F606W$, $F814W$ photometry.

6 SUMMARY

This investigation was undertaken primarily to evaluate the consequences of metal abundance variations on the magnitudes and colours of stars to complement the study by VandenBerg et al. (2012), who determined the effects on predicted luminosities and T_{eff} s of increasing the abundances of several of the most abundant metals, in turn, by 0.4 dex. It was also our intention at the outset to apply our stellar models to the photometry of a few GCs from the recent *HST* UV Legacy Survey (Piotto et al. 2015, Nardiello et al. 2018) in order to assess how well they are able to reproduce observed colours from the UV to the IR over a wide range in $[\text{Fe}/\text{H}]$ and, if possible, to refine our understanding of these systems. The project as a whole has been divided into two parts: this paper, which focuses on the model computations, and Paper II, which compares our isochrones with the observed CMDs of 47 Tuc, NGC 6362, M5, M3, M55, and M92.

This work began with the definition of a dozen mixtures of the metals that assumed either enhanced abundances of individual elements (C, O, Mg, or Si), or variations in the C:N:O abundance ratio for different values of $[\text{CNO}/\text{Fe}]$. For each of the adopted mixtures, we computed (i) MARCS model atmospheres and high-resolution synthetic spectra for suitable ranges in $\log g$, T_{eff} , and $[\text{Fe}/\text{H}]$, (ii) BCs from these spectra for many of the broad-band filters currently in use, including, but not limited to, those for the 2MASS, SDSS, Johnson-Cousins, and the *HST* ACS and WFC3 photometric systems, and (iii) grids of evolutionary tracks for, in most cases, masses in the range $0.10 \leq M/M_{\odot} \leq 1.0$, from which ~ 7 –14 Gyr isochrones could be generated. For masses $\lesssim 0.4M_{\odot}$, the boundary conditions of the stellar interior models were derived from the MARCS model atmospheres at an optical depth $\tau = 100$ in order to make the best possible predictions of stellar temperatures along the lower MS (see the discussion of this point by VandenBerg et al. 2014). A scaled solar T - τ was used to describe the atmospheric structure at higher masses. Importantly, all of the model atmo-

spheres, the synthetic spectra, and the stellar models were computed for exactly the same mixtures of the heavy elements.

Worth emphasizing is that the current version of the MARCS spectral synthesis code contains a number of improvements over the version that was used for the grids published by Gustafsson et al. (2008). In particular, it incorporates an improved treatment of C, N, and O (notably of molecules formed out of these atoms), with important consequences for UV spectra, irrespective of variations in the abundances of these elements are considered. That is, the updated BCs for the $[\alpha/\text{Fe}] = 0.4$ reference mixture differ from those derived by CV14 from 2008 MARCS spectra by amounts that increase systematically with decreasing wavelength (see Fig. 4). (In order to facilitate comparisons with observations, we have produced tables of the updated BCs and the necessary computer codes to transform Victoria-Regina isochrones for $[\alpha/\text{Fe}] = 0.4$, with and without the metal abundance variations that have been considered in this investigation; they may be obtained from the web site that is provided at the end of this paper.)

Our results have demonstrated the necessity of treating the chemical abundances in the atmosphere, interior, and spectrum synthesis models as consistently as possible. In particular, the temperatures of LMS stars are predicted to have a strong dependence on the abundance of oxygen in the atmospheric layers, much more so than in the case of any other metal. This dependence is in the sense that O-rich stellar models are significantly cooler, at a given luminosity, than those without such enhancements or those with depleted oxygen (see Fig. 8). On the other hand, higher O abundances result in, e.g., bluer $M_{F110W} - M_{F160W}$ colours at a fixed T_{eff} and gravity (Fig. 6). Indeed, enhanced O has the net effect of making the LMS portion of an O-rich isochrone considerably bluer on the $M_{F110W} - M_{F160W}$, M_{F606W} diagram than that of an otherwise identical isochrone without the oxygen enhancement (see Fig. 12). Thus, insofar as this particular colour is concerned, O-rich stars are expected to be bluer, despite being cooler. (As shown in Fig. 6, enhanced O can also result in redder colours, depending on the colour index that is considered.)

By contrast, the abundances of Mg or Si are of relatively little consequence for the temperatures of LMS stars (see Fig. 8). These elements are also unlike oxygen in that they have a significant influence on the temperatures of upper MS, TO, and RGB stars (see VandenBerg et al. 2012 and our Fig. 7).⁶ Enhanced Mg or Si results in redder colours along the giant branch (see Fig. 5), which is due partly to their effects on the stellar T_{eff} scale and partly to their impact on bolometric corrections. However, modest variations in the He abundance ($\delta Y \lesssim 0.05$) have larger consequences for the temperatures of upper MS, TO, and RGB stars, particularly at lower metallicities, than Mg and Si.

In fact, He abundance variations, which are known to exist in most GCs, may have more profound implications for our understanding of these systems than the observed CN, ON, ONa, and MgAl anticorrelations. For instance, Gratton et al. (2013) has found that the colours of HB stars are correlated with the abundances of p -capture elements in M5, with decreasing O and increasing Na abundances in the direction from red to blue. Similar findings in M22 (Gratton et al. 2014) and in NGC 6723 (Gratton et al. (2015) led these researchers to conclude that chem-

⁶ It is well known that the luminosities and T_{eff} s of TO stars are dependent on the abundance of oxygen in their deep interiors because of structural changes that occur when the C+N+O abundance is changed, but that is a separate issue.

ical composition (primarily He) is the main driver behind the distributions of stars along the lengths of cluster HBs. This is not a new idea (see, e.g., D’Antona & Caloi 2004), and indeed modern simulations of HB populations (e.g., Denissenkov et al. 2017) provide the best matches to the observed CMD distributions of the core He-burning stars if Y varies by small (~ 0.01 – 0.02) to moderate amounts (~ 0.04 – 0.05), depending on the length of the HB (especially the length of the blue tail). However, as already noted in § 1, the He abundance variations that have been derived from chromosome maps (Milone et al. 2018) are sometimes in rather poor agreement with other determinations.

We concur with the results of Pietrinferni et al. (2009), who showed that isochrones for upper MS, TO, and RGB stars are independent of differences in the C:N:O abundance ratio, provided that $C+N+O = \text{constant}$. Indeed, even along the LMS, variations in C:N remain inconsequential, which follows from the fact that model atmospheres predict nearly identical properties (e.g., pressure, temperature) at $\tau = 100$ for the base a4s21 mix, which is relevant to CN-weak stars, and for the a4CN mixture, which has C and N abundances that are more characteristic of CN-strong stars. Since the MARCS atmospheres are used as boundary conditions, the isochrones for these two cases superimpose one another almost exactly on the theoretical plane. As a result, there is no need to compute evolutionary tracks and isochrones for different C:N ratios. One can simply apply the BCs for, e.g., the a4CN mixture to the isochrones for the a4s21 mix for the same values of $[\alpha/\text{Fe}]$ and $[\text{CNO}/\text{Fe}]$ in order to determine how predicted magnitudes and colours are affected by the variations in CN. The same point has been made by Pietrinferni et al.

As first shown by Sbordone et al. (2011), broad-band colours are quite sensitive to the abundances of C and N, particularly at shorter wavelengths. Our calculations, which considered the range in $[\text{Fe}/\text{H}]$ from -2.5 to -0.5 , while Sbordone et al. examined models for just a single metallicity, similarly predict that increased N abundances will result in redder $U-B$ or $M_{F336} - M_{F438}$ colours — especially along the giant branch, but also along the MS if the metallicity is sufficiently high; see, e.g., Fig. 10. The same figure shows that enhanced C abundances will cause redder $M_{F438W} - M_{F606W}$ colours and bluer $M_{F336W} - M_{F438W}$ colours. As our exploratory study was limited to just a single variation of the C:N and O:N abundance ratios, though for two values of $[\text{CNO}/\text{Fe}]$, it would undoubtedly be worthwhile to map out the dependence of broad-band colours along the observed C–N and O–N anticorrelations in much finer detail. Nevertheless, despite the limitations of our models, they appear to be reasonably successful in explaining the distributions of CN-weak and CN-strong stars in GCs. This is demonstrated in Paper II, which also presents some evidence in support of the possibility that these systems contain C-enhanced stellar populations ($[\text{C}/\text{Fe}] \gtrsim 0.5$).

ACKNOWLEDGEMENTS

We are indebted to Kjell Eriksson for the calculations that he carried out to examine the dependence of synthetic spectra on the assumed model atmosphere structures and for valuable discussions on this issue. We also thank Poul Erik Nissen and Anish Amarsi for their careful readings of our paper, which resulted in a number of improvements, and Pavel Denisenkov, John Norris, and David Yong for helpful comments and/or useful references to published work. LC is the recipient of the ARC Future Fellowship FT160100402.

DATA AVAILABILITY

Stellar evolutionary grids that are the basis of the isochrones that appear in Figs. 4–9, along with the computer codes (in FORTRAN) that were used to generate the isochrones on both the theoretical and observed planes are contained in the file `vecf.zip` which may be downloaded from <https://www.canfar.net/storage/list/VRmodels>. Codes are also provided to evaluate (i) the effects on BCs of varying the micro-turbulent velocity and the helium mass-fraction abundance, Y , and (ii) the differences in the BCs for different mixtures of the metals relative to those for any user-selected reference mix at the grid values of $\log g$, T_{eff} , and $[\text{Fe}/\text{H}]$. A description of the contents of the zip file and instructions on how to run the various FORTRAN codes are given in `vecf_readme`. This is the only other file pertaining to the current project that should be downloaded.

REFERENCES

- Abbas, M. A., Layden, C., Guldenschuh, K. A., et al. 2015, *AJ*, 149, 40
- Akima, H. 1970, *J. Assoc. Comput. Mach.*, 17, 589
- Asplund, M., Grevesse, N., Sauval, A. J., & Scott, P. 2009, *ARAA*, 47, 481
- Bellini, A., Milone, A. P., Anderson, J., et al. 2017, *ApJ*, 844, 164
- Beom, M., Na, C., Ferguson, J. W., & Kim, Y.-C. 2016, *ApJ*, 826, 155
- Bonifacio, P., Caffau, E., Ludwig, H.-G., et al. 2018, *A&A*, 611, A68
- Briley, M. M., Cohen, J. G., & Stetson, P. B. 2004, *AJ*, 127, 1579
- Brogaard, K., VandenBerg, D. A., Bruntt, H., et al. 2012, *A&A*, 543, A106
- Brogaard, K., VandenBerg, D. A., Bedin, L. R., Milone, A. P., Thygesen, A., & Grundahl, F. 2017, *MNRAS*, 468, 645
- Brown, J. A., & Wallerstein, G. 1992, *AJ*, 104, 1818
- Cannon, R. D., Croke, B. F. W., Bell, R. A., Hesser, J. E., & Stathakis, R. A. 1998, *MNRAS*, 298, 601
- Carbon, D. F., Langer, G. E., Butler, D., et al. 1982, *ApJS*, 49, 207
- Carretta, E., Bragaglia, A., Gratton, R. G., D’Orazi, V., & Lucatello, S. 2009a, *A&A*, 508, 695
- Carretta, E., Bragaglia, A., Gratton, R. G., et al. 2009b, *A&A*, 508, 695
- Carretta, E., Bragaglia, A., Gratton, R. G., Lucatello, S., & D’Orazi, V. 2012, *ApJ*, 750, L14
- Carretta, E., Bragaglia, A., Gratton, R. G., et al. 2014, *A&A*, 564, A60
- Carretta, E., Bragaglia, A., Lucatello, S., Gratton, R. G., D’Orazi, V., & Solima, A. 2018, *A&A*, 615, A17
- Carretta, E., Gratton, R. G., Lucatello, S., Bragaglia, A., & Bonifacio, P. 2005, *A&A*, 433, 597
- Casagrande, L., Ramírez, I., Meléndez, J., Bessell, M., & Asplund, M. 2010, *A&A*, 512, 54
- Casagrande, L., & VandenBerg, D. A. 2014, *MNRAS*, 444, 392 (CV14)
- Cassisi, S., Mucciarelli, A., Pietrinferni, A., Salaris, M., & Ferguson, J. W. 2013, *A&A*, 544, A19
- Cassisi, S., Salaris, M., Castelli, F., & Pietrinferni, A. 2004, *ApJ*, 616, 498
- Chiavassa, A., Casagrande, L., Collet, R., Magic, Z., Bigot, L., Thévenin, F., & Asplund, M. 2018, *A&A*, 611, A11
- Cohen, J. G. 1978, *ApJ*, 223, 487

- Cohen, J. G., Briley, M. M., & Stetson, P. B. 2002, *AJ*, 123, 2525
- Cohen, J. G., Briley, M. M., & Stetson, P. B. 2005, 130, 1117
- Correnti, M., Gennaro, M., Kalirai, J. S., Brown, T. M., & Calamida, A. 2016, *ApJ*, 823, 18
- Correnti, M., Gennaro, M., Kalirai, J., Cohen, R. E., & Brown, T. M. 2018, *ApJ*, 864, 147
- D'Antona, F., & Caloi, V. 2004, *ApJ*, 611, 871
- Denissenkov, P. A., VandenBerg, D. A., Kopacki, G., & Ferguson, J. W. 2017, *ApJ*, 849, 159
- Denissenkov, P. A., & VandenBerg, D. A. 2003, *ApJ*, 593, 509
- Denissenkov, P. A., & Weiss, A. 2004, *ApJ*, 603, 119
- Di Cecco, A., Bono, G., Prada Moroni, P. G., et al. 2015, *AJ*, 150, 51
- Dotter, A., Chaboyer, B., Ferguson, J. W., et al. 2007, *ApJ*, 666, 403
- Dotter, A., Conroy, C., Cargile, P., & Asplund, M. 2017, *ApJ*, 840, 99
- Drake, J. J., Smith, V. V., & Suntzeff, N. B. 1992, *ApJ*, 395, L795
- Edvardsson, B. 2008, *Phys. Scr.*, T133, 014011
- Edvardsson, B., Andersen, J., Gustafsson, B., Lambert, D. L., Nissen, P. E., & Tonkin, J. 1993, *A&A*, 275, 101
- Fabbian, D., Nissen, P. E., Asplund, M., Pettini, M., & Akerman, C. 2009, *A&A*, 500, 1143
- Ferguson, J. W., Alexander, D. R., Allard, F., et al. 2005, *ApJ*, 623, 585
- Friel, E. D., & Geisler, D. 1991, *AJ*, 101, 1338
- Girardi, L., Castelli, F., Bertelli, G., & Nasi, E. 2007, *A&A*, 468, 657
- Gratton, R. G., Bonifacio, P., Bragaglia, A., et al. 2001, *A&A*, 369, 87
- Gratton, R. G., Lucatello, S., Sollima, A., et al. 2013, *A&A*, 549, A41
- Gratton, R. G., Lucatello, S., Sollima, A., et al. 2014, *A&A*, 563, A13
- Gratton, R. G., Lucatello, S., Sollima, A., et al. 2015, *A&A*, 573, A92
- Grevesse, N., Asplund, M., & Sauval, A. J. 2007, *SSRv*, 130, 105
- Gustafsson, B., Edvardsson, B., Eriksson, K., Jorgensen, U. G., Nordlund, Å., & Plez, B. 2008, *A&A*, 486, 951
- Herwig, F., VandenBerg, D. A., Navarro, J. F., Ferguson, J. W., & Paxton, B. 2012, *ApJ*, 757, 132
- Hesser, J. E. 1978, *ApJ*, 223, L117
- Hesser, J. E., & Bell, R. A. 1980, *ApJ*, 238, L149
- Holweger, H., & Mueller, E. A. 1974, *Sol. Phys.*, 39, 19
- Iglesias, C. A., & Rogers, F. J. 1996, *ApJ*, 464, 943
- King, I. R., Bedin, L. R., Cassisi, S., et al. 2012, *AJ*, 144, 5
- Kraft, R. P. 1994, *PASP*, 106, 553
- Kurucz, R. L. 2005, *Mem.Soc.Astron.Ital.Suppl.*, 8, 76
- Kurucz, R. L. 2014, In "Determination of the Atmospheric Parameters of B-, A-, F-, and G-Type Stars", eds. E. Niemczura, B. Smalley, & W. Pych (Springer Cham), 39
- Martins, F., Chantreau, W., & Charbonnel, C. 2017, *SF2A: Proc. Annual Meeting of the French Society of Astronomy & Astrophysics*, eds. C. Reyl , P. D. Matteo, F. Herpin, E. Langade, A. Lançon, Z. Meliani, & F. Royer, 57
- Massari, D., Fiorentino, G., McConnachie, A., et al. 2016, *A&A*, 586, A51
- Milone, A. P., Marino, A. F., Piotto, G., et al. 2015a, *ApJ*, 808, 51
- Milone, A. P., Marino, A. F., Piotto, G., et al. 2015b, *MNRAS*, 447, 927
- Milone, A. P., Marino, A. F., Bedin, L. R., et al. 2017, *MNRAS*, 469, 800
- Milone, A. P., Marino, A. F., Bedin, L. R., et al. 2019, *MNRAS*, 484, 4046
- Milone, A. P., Marino, A., Renzini, A., et al. 2018, *MNRAS*, 481, 5098
- Nardiello, D., Libralato, M., Piotto, G., et al. 2018, *MNRAS*, 481, 3382
- Nissen, P. E., Chen, Y. Q., Carigi, L., Schuster, W. J., & Zhao, G. 2014, *A&A*, 568, A25
- Norris, J., Cottrell, P. L., Freeman, K. C., & Da Costa, G. S. 1981, *ApJ*, 244, 205
- Norris, J. E., & Da Costa, G. S. 1995, *ApJ*, 447, 680
- Norris, J., & Pilachowski, C. A. 1985, *ApJ*, 299, 295
- Osborn, W. 1971, *Obs.*, 91, 223
- Paxton, B., Bildsten, L., Dotter, A., Herwig, F., Lesaffre, P., & Timmes, F. 2011, *ApJS*, 192, 3
- Pereira, T. M. D., Asplund, M., Collet, R., Thaler, I., Trampedach, R., & Leenaarts, J. 2013, *A&A*, 554, A118
- Peterson, R. C. 1980, *ApJ*, 237, L87
- Pietrinferni, A., Cassisi, S., Salaris, M., & Castelli, F. 2006, *ApJ*, 642, 797
- Pietrinferni, A., Cassisi, S., Salaris, M., Percival, S., & Ferguson, J. W. 2009, *ApJ*, 697, 275
- Pilachowski, C. A. 1988, *ApJ*, 326, L57
- Pilachowski, C. A. 1989, in *The Abundance Spread Within Globular Clusters*, ed. G. C. Cayrel de Strobel, M. Spite, & T. L. Evans (Obs. de Paris, Paris), 1
- Piotto, G., Milone, A. P., Bedin, L. R., et al. 2015, *AJ*, 149, 91
- Piotto, G., Villanova, S., Bedin, L. R., et al. 2005, *ApJ* 621, 777
- Popper, D. M. 1947, *ApJ*, 105, 204
- Pulone, L., De Marchi, G., Covino, S., & Paresce, F. 2003, *A&A*, 399, 121
- Ram rez, S.V., & Cohen, J. G. 2003, *AJ*, 125, 224
- Richard, O., Michaud, G., Richer, J., Turcotte, S., Turck-Chi ze, S., & VandenBerg, D. A. 2002, *ApJ*, 568, 979
- Rood, R. T., & Crocker, D. A. 1985, in *Production and Distribution of C, N, O Elements*, ed. I. J. Danziger, F. Matteucci, & K. Kj r (Garching: ESO), 61
- Salaris, M., Chieffi, A., & Straniero, O. 1993, *ApJ*, 414, 580
- Salaris, M., Weiss, A., Ferguson, J. W., & Fusilier, D. J. 2006, *ApJ*, 645, 1131
- Saracino, S., Dalessandro, E., Ferraro, F. R., et al. 2018, *ApJ*, 860, 95
- Sarajedini, A., Bedin, L. R., Chaboyer, B., et al. 2007, *AJ*, 133, 1658
- Sbordone, L., Salaris, M., Weiss, A., & Cassisi, S. 2011, *A&A*, 534, A9
- Schlegel, D., Finkbeiner, D. P., & Davis, M. 1998, *ApJ*, 500, 525
- Shetrone, M. D. 1996a, *AJ*, 112, 1517
- Shetrone, M. D. 1996b, *AJ*, 112, 2639
- Smith, G. H. 1987, *PASP*, 99, 67
- Smith, G. H., Briley, M. M., & Harbeck, D. 2005, *AJ*, 129, 1589
- Smith, G. H., Shetrone, M. D., Bell, R. A., Churchill, C. W., & Briley, M. M. 1996, *AJ*, 112, 1511
- Snedden, C., Kraft, R. P., Prosser, C. F., & Langer, G. E. 1991, *AJ*, 102, 2001
- Tailo, M., D'Antona, F., Caloi, V., et al. 2019, *MNRAS*, 486, 5895
- VandenBerg, D. A. 1992, *ApJ*, 391, 685
- VandenBerg, D. A., Bergbusch, P. A., Dotter, A., Ferguson, J. W., Michaud, G., Richer, J., & Proffitt, C. R. 2012, *ApJ*, 755, 15
- VandenBerg, D. A., Bergbusch, P. A., Ferguson, J. W., & Edvardsson, B. 2014a, *ApJ*, 794, 72
- VandenBerg, D. A., Brogaard, K., Leaman, R., & Casagrande,

- L. 2013, ApJ, 775, 134 (VBLC13)
VandenBerg, D. A., Casagrande, L., & Stetson, P. B. 2010, AJ, 140, 1020
VandenBerg, D. A., & Denissenkov, P. A. 2018, ApJ, 862, 72
VandenBerg, D. A., Denissenkov, P. A., & Catelan, M. 2016, ApJ, 827, 2
VandenBerg, D. A., & Poll, H. E. 1989, AJ, 98, 1451
VandenBerg, D. A., Richard, O., Michaud, G., & Richer, J. 2002, ApJ, 571, 487
VandenBerg, D. A., Swenson, F. J., Rogers, F. J., Iglesias, C. A., & Alexander, D. R. 2000, ApJ, 532, 430
Yong, D., Grundahl, F., Lambert, D. L., Nissen, P. E., & Shetrone, M. D. 2003, A&A, 402, 985
Yong, D., Grundahl, F., Nissen, P. E., Jensen, H. R., & Lambert, D. L. 2005, A&A, 438, 875
Yong, E., Aoki, W., & Lambert, D. L. 2006, ApJ, 638, 1018
Zennaro, M., Milone, A. P., Marino, A. F., Cordini, G., Lagioia, E. P., & Tailo, M. 2019, MNRAS, 487, 3239

This paper has been typeset from a $\text{\TeX}/\text{\LaTeX}$ file prepared by the author.